



RESEARCH ARTICLE

10.1029/2018TC005219

Special Section:

Geodynamics, Crustal and Lithospheric Tectonics, and active deformation in the Mediterranean Regions (A tribute to Prof. Renato Fuciniello)

Key Points:

- We present a melt inclusion study of recent primitive Anatolian intraplate magmas at Kula, Ceyhan-Osmaniye, and Karacadağ
- Studied magmas indicate mixing of two primary melt components, which reflect asthenospheric and lithospheric mantle sources
- Anatolian intraplate magmatism seems to be triggered by large-scale mantle flow that also affects the wider Arabian and North African region

Supporting Information:

- Supporting Information S1
- Table S1

Correspondence to:

I. K. Nikogosian,  
i.nikogosian@vu.nl

Citation:

Nikogosian, I. K., Bracco Gartner, A. J. J., van Bergen, M. J., Mason, P. R. D., & van Hinsbergen, D. J. J. (2018). Mantle sources of recent Anatolian intraplate magmatism: A regional plume or local tectonic origin?. *Tectonics*, 37, 4535–4566. <https://doi.org/10.1029/2018TC005219>

Received 30 JUN 2018

Accepted 21 NOV 2018

Accepted article online 28 NOV 2018

Published online 15 DEC 2018

©2018. The Authors.

This is an open access article under the terms of the Creative Commons Attribution-NonCommercial-NoDerivs License, which permits use and distribution in any medium, provided the original work is properly cited, the use is non-commercial and no modifications or adaptations are made.

# Mantle Sources of Recent Anatolian Intraplate Magmatism: A Regional Plume or Local Tectonic Origin?

I. K. Nikogosian<sup>1,2</sup> , A. J. J. Bracco Gartner<sup>1,2</sup> , M. J. van Bergen<sup>2</sup> , P. R. D. Mason<sup>2</sup> , and D. J. J. van Hinsbergen<sup>2</sup> 

<sup>1</sup>Department of Earth Sciences, Vrije Universiteit Amsterdam, Amsterdam, The Netherlands, <sup>2</sup>Department of Earth Sciences, Utrecht University, Utrecht, The Netherlands

Abstract

We present an extensive study of rehomogenized olivine-hosted melt inclusions, olivine phenocrysts, and chromian spinel inclusions to explore the link between geodynamic conditions and the origin and composition of Pliocene–Quaternary intraplate magmatism in Anatolia at Kula, Ceyhan-Osmaniye, and Karacadağ. Exceptional compositional variability of these products reveals early and incomplete mixing of distinct parental melts in each volcanic center, reflecting asthenospheric and lithospheric mantle sources. The studied primitive magmas consist of (1) two variably enriched ocean island basalt (OIB)-type melts in Kula; (2) both OIB-type and plume mid-ocean ridge basalt (P-MORB)-like melts beneath Toprakkale and Üçtepel (Ceyhan-Osmaniye); and (3) two variably enriched OIB-type melts beneath Karacadağ. Estimated conditions of primary melt generation are 23–9 kbar, 75–30 km, and 1415–1215 °C for Kula; 28–19 kbar, 90–65 km, and 1430–1350 °C for Toprakkale; 23–18 kbar, 75–60 km, and 1400–1355 °C for Üçtepel; and 35–27 kbar, 115–90 km, and 1530–1455 °C for Karacadağ, the deepest levels of which correspond to the depth of the lithosphere-asthenosphere boundary in all regions. Although magma ascent was likely facilitated by local deformation structures, recent Anatolian intraplate magmatism seems to be triggered by large-scale mantle flow that also affects the wider Arabian and North African regions. We infer that these volcanics form part of a much wider Arabian-North African intraplate volcanic province, which was able to invade the Anatolian upper plate through slab gaps.

## 1. Introduction

Neogene–Quaternary silica-undersaturated alkaline volcanics in Anatolia, a central segment of the 7,000-km-long Alpine-Himalayan orogenic belt, are surprising in context of the widely inferred geodynamic conditions during and following continental collision of the African Arabian and Eurasian plates. The late Cenozoic tectonic evolution of the eastern Mediterranean region has been dominated by the northward subduction of the Neotethyan oceanic lithosphere along the Hellenic arc in the west and continental collision along the Bitlis-Zagros suture zone in the east (Taymaz et al., 2007), in which major structures, such as the Aegean-Cyprus arc system, the North and East Anatolian Fault Zones and the Dead Sea Fault Zone (Westaway, 1994; Westaway & Arger, 1996), have played a key role. This setting of long-term subduction and collision would be logically associated with widespread arc volcanism, but in several locations in Anatolia, primitive intraplate-type volcanics are found, which are difficult to reconcile with subduction (e.g., Aldanmaz et al., 2006; Çoban, 2007; Dilek & Altunkaynak, 2007; Keskin, 2007). Upper Neogene intraplate-type volcanics are found in several places in western and eastern Anatolia and occur throughout different styles of tectonic provinces, from extensional in western Anatolia to transpressional and transcurrent in eastern, northern, and central Anatolia (Şengör et al., 1985; Şengör & Yilmaz, 1981). Such types of volcanics are often associated with mantle plumes, but no such plume appears to be present below Anatolia, nor is evident from the young volcanic’s petrogenesis (e.g., Aldanmaz et al., 2000, 2006; Arger et al., 2000; Ekici et al., 2012, 2014; McKenzie & O’Nions, 1995; Pearce et al., 1990; Polat et al., 1997), although large-scale mantle flow associated with the distant Afar plume may have played a role (Faccenna et al., 2013).

Long-term, northwestern Anatolian Oligo-Miocene volcanism is interpreted to have resulted from melting of a metasomatized Neotethyan lithospheric mantle wedge, perhaps aided by lithospheric delamination or slab breakoff and concomitant asthenospheric upwelling (Aldanmaz et al., 2000; Chakrabarti et al., 2012; Dilek & Altunkaynak, 2007). Western Anatolian volcanic sources are thought to have transitioned from a subduction-modified lithospheric mantle to the upwelling of ocean island basalt (OIB)-like asthenospheric

mantle, possibly aided by lithospheric extension (e.g., Aldanmaz et al., 2000; Güleç, 1991; Seyitoğlu et al., 1997). This OIB-like asthenosphere may leak through a vertical tear in the subducted African slab (Berk Biryol et al., 2011; Chakrabarti et al., 2012; van Hinsbergen, Kaymakci, et al., 2010; Jolivet et al., 2015; Klaver et al., 2016).

In central southern Anatolia, mantle sources of young volcanics on the shores of the İskenderun Gulf are also thought to resemble an OIB-like asthenosphere (Alıcı et al., 2001; Parlak et al., 2000, 1998, 1997; Polat et al., 1997; Yurtmen et al., 2000), variously enriched by subduction-related metasomatism (Bağcı et al., 2011; Italiano et al., 2017; Polat et al., 1997; Yurtmen et al., 2000). Upwelling and decompressional melting has in this region been inferred to relate to transtensional tectonics associated with the East Anatolian Fault and oblique eastern Cyprus trench (Bağcı et al., 2011; Italiano et al., 2017; Parlak et al., 2000; Polat et al., 1997) and, further south, to the Dead Sea Fault Zone which runs into Syria (Ma et al., 2011).

Finally, Miocene–Quaternary magmatism in the Karacadağ Volcanic Complex in southeastern Anatolia, on the Arabian foreland, has been interpreted to be the result of asthenospheric mantle upwelling and melting beneath the attenuated Arabian plate, with a possible minor role for restricted local extension, as it migrated northward during the Neogene (Ekici et al., 2012, 2014; Elitok & Dolmaz, 2008; Keskin et al., 2012a; Pearce et al., 1990). Its OIB-like mantle source (Lustrino et al., 2012; Şen et al., 2004), which is distinct from that of magmatism attributed to the Afar plume (Ekici et al., 2012, 2014), is inferred to be metasomatized and compositionally heterogeneous (Lustrino et al., 2012; Pearce et al., 1990).

In summary, Late Neogene alkaline volcanism is interpreted to result from very different local tectonic and geodynamic processes throughout Anatolia. Previous studies of Anatolian intraplate volcanics have predominantly used bulk-rock geochemical and isotope data (e.g., Aldanmaz et al., 2006; Alıcı et al., 2001, 2002; Arger et al., 2000; Bağcı et al., 2011; Chakrabarti et al., 2012; Ekici et al., 2012, 2014; Italiano et al., 2017; Klaver et al., 2016; Lustrino et al., 2012; Polat et al., 1997; Sölpüker, 2007; Yurtmen et al., 2000) to investigate the generation of alkaline magmas across various tectonic settings. However, in view of the complex history of the region following late-stage subduction or collision of the African, Eurasian, and Arabian plates, the nature and interaction of mantle and subduction components are difficult to decipher using bulk-rock geochemistry alone. Instead, olivine-hosted melt inclusions (MI) may provide information on primitive magma compositions in substantially more detail and shed light on the compositional diversity of minor volumes of primary melts with compositions not represented by erupted products (e.g., Danyushevsky, Sokolov, et al., 2002; Jackson & Hart, 2006; Koornneef et al., 2015; Maclennan, 2008; Nikogosian et al., 2016; Nikogosian & van Bergen, 2010; Saal et al., 1998; Schiano et al., 2004; Sobolev, 1996).

Here we use MI data to explore the link between geodynamic conditions and the origin and composition of intraplate magmatism with alkaline affinities in Anatolia. We follow the Tethys suture between Europe and Africa-Arabia, covering key late Neogene–Quaternary volcanic centers in western Anatolia (Kula), in central southern Anatolia near the triple junction of the African, Arabian, and Anatolian plates (Ceyhan-Osmaniye), and on the Arabian foreland (Karacadağ). The main aim of this study is to (1) determine the compositions of (near-)primary melts that gave rise to Pliocene–Quaternary intraplate magmatism in Anatolia; (2) estimate pressure and temperature conditions of melting; (3) characterize possible mantle source components that generated contemporaneous OIB-like end-members across contrasting geodynamical settings; and (4) place their origin in the regional geodynamic context.

## 2. Geodynamic and Magmatic Setting

The present-day plate boundary between the Eurasian, African, and Arabian plates (Figure 1) corresponds to the western segment of the Alpine-Himalayan orogenic belt. Three processes are generally invoked to explain the late Cenozoic evolution of the eastern Mediterranean region: (i) the Arabia-Eurasia plate collision along the Bitlis-Taurides collisional belt since the early to late Miocene (Faccenna et al., 2006; Hüsing et al., 2009; Okay et al., 2010); (ii) the postcollisional westward escape of the Anatolian block from the Arabia-Eurasia collision zone, facilitated by the North and East Anatolian fault systems (e.g., Şengör et al., 1985; Şengör & Yilmaz, 1981); and (iii) the ongoing northward subduction of the African plate beneath Eurasia along the Hellenic and Cyprus Trenches (Berk Biryol et al., 2011; Meulenamp et al., 1988).

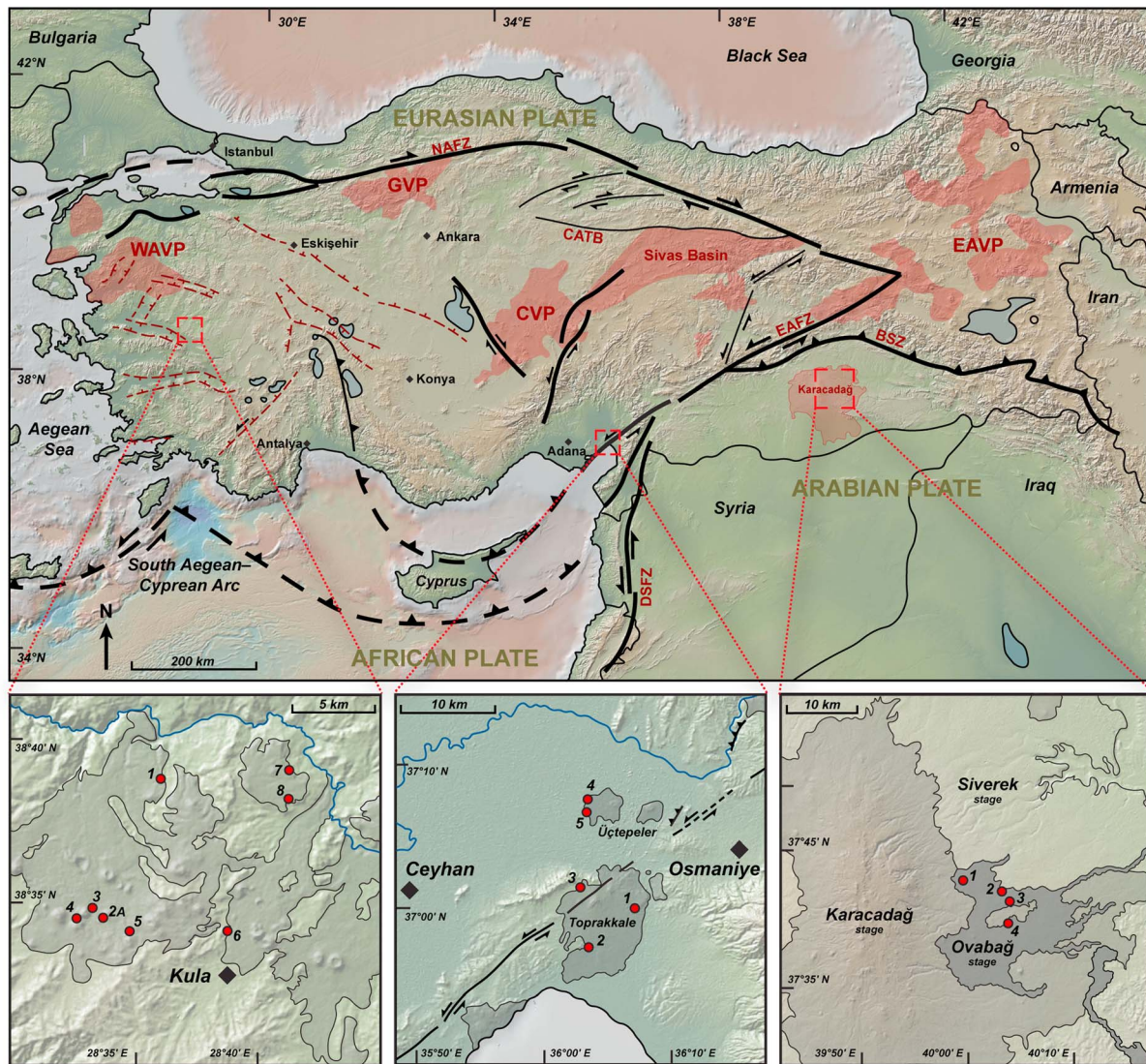


**Figure 1.** Tectonic map of the Anatolian sector of the Alpine-Himalayan orogenic belt. Insets show simplified maps of the studied Anatolian volcanic centers of Kula, Ceyhan-Osmaniye, and Karacadağ, with sample locations indicated by red dots (respective prefixes KUL-, OSM-, and KAR- have been omitted for clarity). Black half arrows indicate motion directions along strike-slip faults. Major volcanic provinces include the Western Anatolian Volcanic Province (WAVP), Galatean Volcanic Province (GVP), Cappadocian Volcanic Province (CVP), and East Anatolian Volcanic Province (EAVP). Major tectonic features include the North Anatolian Fault Zone (NAFZ), Central Anatolian Thrust Belt (CATB), East Anatolian Fault Zone (EAFZ); Bitlis Suture Zone (BSZ), and Dead Sea Fault Zone (DSFZ). Maps compiled from Ekici et al. (2014), Holness and Bunbury (2006), Koçbulut et al. (2013), Ryan et al. (2009), and Yurtmen et al. (2000).

In western Anatolia, Aegean slab rollback inferred to have caused late Eocene and younger extension is thought to have been associated with lithospheric delamination (Dilek et al., 2009; van Hinsbergen, Kaymakci, et al., 2010). The onset of extension is inferred to be ~45 Ma (Brun & Sokoutis, 2010) and stretched previously accreted nappes that accreted during long-term subduction of oceanic and microcontinental lithosphere (Jolivet & Brun, 2010; van Hinsbergen et al., 2005; van Hinsbergen & Schmid, 2012). Magmatism summarized as “postcollisional” in western Anatolia followed Paleogene continental subduction and ranges from 37.3 Ma (Ercan et al., 1995) to recent times (~0.026 Ma; Richardson-Bunbury, 1996). Western Anatolian postcollisional magmatism has occurred in several compositionally distinct phases and may have been controlled by mantle lithosphere delamination, slab breakoff, and asthenospheric upwelling and decompression melting, reflecting the eastern Mediterranean geodynamic evolution during the Cenozoic (Dilek & Altunkaynak, 2007). Volcanism that evolved during the shift in tectonic regime from N-S directed compression and nappe accretion to N-S directed extension in the Oligocene to early Miocene (e.g.,

Gessner et al., 2013; van Hinsbergen, 2010) shifted from calc-alkaline with mostly mafic-intermediate and felsic products (late Oligocene–early Miocene) to predominantly mafic, alkaline compositions (late Miocene; Aldanmaz et al., 2000; Güleç, 1991; Seyitoğlu et al., 1997).

In contrast, eastern Anatolia has been governed by collision of Arabia with the Anatolian and Eurasian blocks (Allen et al., 2004; McQuarrie & van Hinsbergen, 2013). During the Paleocene, the area was still associated with widespread Neotethyan oceanic lithosphere subduction beneath and within the modern Anatolian orogen (Gürer & van Hinsbergen, 2018), which terminated with collision at the Bitlis suture at ~18–11 Ma (Hüsing et al., 2009; Okay et al., 2010), generating the eastern Anatolian high plateau (Figure 1; Dewey et al., 1986; Şengör et al., 2008; Şengör & Kidd, 1979). Magmatic activity and crustal thickening were induced by strong N-S compression since the early Miocene (Dewey et al., 1986), but eastern Anatolian volcanism was particularly extensive after collision (11.4 Ma to present). The geochemistry of these lavas varies significantly in N-S direction, from calc-alkaline rocks from the Erzurum-Kars Plateau and Mt. Ararat in the north, indicating an enriched mantle source with a distinct subduction signature, via transitional products from Bingöl and Süphan (Pearce et al., 1990), to the alkaline to mildly alkaline rocks from the Muş-Nemrut-Tendürek volcanoes in the south, which show a dominant intraplate signature (Keskin, 2003). The apparent southward decrease in subduction signature follows a temporal trend: Volcanic activity initiated in the north, approximately coeval with the rapid regional block uplift at ~13–11 Ma, and migrated southward over time (Keskin, 2007). The temporal and spatial geochemical variations, coupled with the uplift history and volcanic ages in the Eastern Anatolian Collision Zone, have been linked to mechanical removal of the mantle lithosphere by delamination beneath the Erzurum-Kars Plateau in the north (Keskin, 2007; Keskin et al., 1998; Pearce et al., 1990) and slab steepening and breakoff beneath a subduction-accretion complex in the south (Keskin, 2003; Şengör et al., 2003).

Volcanism in eastern Anatolia did not remain restricted to the collisional orogen but also occurs on the foreland. Arabian magmatic activity is predominantly intraplate in nature and expressed in several basaltic volcanic fields exhibiting alkaline characteristics. Intraplate magmatism was active from 30 to 16 Ma and from 13 to 8 Ma in southern Turkey (e.g., Karacadağ, Gaziantep, and Kilis; Ekici et al., 2012, 2014; Gürsoy et al., 2009; Lustrino et al., 2010, 2012), northwestern Syria (e.g., Al Ghab and Homs regions; Krienitz et al., 2006; Lustrino & Sharkov, 2006; Ma et al., 2011), and southern Syria/Jordan (Harrat Ash Shaam; Krienitz et al., 2007; Shaw et al., 2003), increasingly so since the Pliocene (Ilani et al., 2001). Most volcanism occurred in close proximity to tectonic structures such as the Dead Sea Fault Zone, Esdraelon Valley, Euphrates Graben, Sirhan Graben, and Karak Graben (Ekici et al., 2014). On the Arabian platform, contemporaneous with the uplift of the eastern Anatolian-Iranian high plateau, the collision also resulted in N-S trending “impactogens” (rift systems striking at high angles to collision-type orogenic belts). Some of these structures (e.g., Akçakale Graben) are thought to be an indicator of E-W extension, although these rifts appear to act, at least partly, as transfer structures between the outer thrusts of the Arabian foreland (Pearce et al., 1990).

Finally, near the triple junction between the African, Arabian, and Anatolian plates, in a complex tectonic regime involving the East Anatolian Fault Zone, the Karasu Fault Zone, and the northern segment of the Dead Sea Transform Fault Zone (Figure 1; Gürsoy et al., 2003; Mahmoud et al., 2013; Meghraoui et al., 2011; Muehlberger, 1981; Tatar et al., 2004), several tectonic basins with volcanic fields have developed. The Miocene–Quaternary İskenderun Basin, located to the west of the Amanos High, and the Amik Basin, in the southern part of the Karasu Rift, have developed in the triple junction area during the early Miocene–early Pliocene, and during strike-slip deformation that became particularly well-developed in Pliocene–Quaternary times (Koç & Kaymakçı, 2013; Robertson et al., 2004). This evolution was accompanied by widespread alkaline volcanism in the region onshore the İskenderun Gulf during the Quaternary (Alıcı et al., 2001; Arger et al., 2000; Bağcı et al., 2011; Italiano et al., 2017; Parlak et al., 1998, 2000; Polat et al., 1997; Rojay et al., 2001; Yurtmen et al., 2000).

### 2.1. Kula

The Kula volcanic field is located in western Anatolia, in the northern part of the Menderes massif (Figure 1). In the Kula volcanic field, lavas were emplaced along active normal faults associated with the E-W trending Alaşehir graben, one of the main E-W trending structures that developed under the late Miocene–Quaternary N-S extensional regime in western Anatolia (Alıcı et al., 2002; Yılmaz et al., 2000). The Kula volcanics represent the youngest magmatic activity in the region (1.9–0.026 Ma; Grützner et al., 2013;

Maddy et al., 2015, 2017; Richardson-Bunbury, 1996), with the main phase of volcanic activity having started at ~0.2 Ma (Bunbury et al., 2001). In contrast to the older, surrounding volcanics regions in western Anatolia, which are dominated by potassium-rich magmas with typically orogenic signatures (e.g., Ersoy et al., 2012; Innocenti et al., 2005; Lustrino & Wilson, 2007; Prelević et al., 2012), the Quaternary Kula volcanics form a primitive, silica-undersaturated Na-alkaline suite (Alici et al., 2002; Richardson-Bunbury, 1996; Tokçaer et al., 2005) and are generally relatively unevolved ( $MgO = 4\text{--}8\text{ wt\%}$ ; Innocenti et al., 2005).

Three different volcanic stages are distinguished within the Kula volcanic province, based on geomorphological differences and geochronological data (e.g., Bunbury et al., 2001; Ercan, 1993; Richardson-Bunbury, 1996; Westaway et al., 2004). In order of decreasing age, these stages are referred to as the Burgaz, Elekçitepe, and Divlittepe stages (Ercan, 1982). The main phase of volcanic activity in the Kula region is represented by the Elekçitepe stage, which may be tied to a significant increase in extensional activity (Ercan, 1993, and references therein). Compositionally, Divlittepe and Burgaz lavas are indistinguishable, whereas Elekçitepe lavas exhibit much greater variation, with generally higher average  $Mg\# [Mg/(Mg + Fe^{2+})]$  and lower  $SiO_2$  and total alkali content (Alici et al., 2002), in line with the former two being generally more fractionated than the Elekçitepe volcanics (Holness & Bunbury, 2006). All these volcanic stages are represented by the eight rock samples that we collected from the Kula volcanic field (Figure 1).

## 2.2. Ceyhan-Osmaniye

The Ceyhan-Osmaniye volcanic field is located in central southern Anatolia (Adana province), onshore the Iskenderun Gulf, close to the triple junction between the African and Arabian plates and the Anatolian block (Figure 1). The basaltic fields of the Ceyhan-Osmaniye region and Karasu Rift are considered to be related to syncollisional transtensional deformation (Polat et al., 1997; Şengör, 1987), wherein magma ascent may have been facilitated by translithospheric fault systems, such as the Karatas-Osmaniye Fault Zone—the southwestward extension of the East Anatolian Fault Zone (Figure 1; Italiano et al., 2017; Polat et al., 1997; Yurtmen et al., 2002). The Ceyhan-Osmaniye volcanic field contains two volcanic centers from which five samples were collected: the Üçtepeler (ÜÇT) and Toprakkale (TOP) volcanoes (Figure 1). K-Ar age determinations place the volcanism in the range of ~2.3 to 0.6 Ma (Arger et al., 2000), similar to other volcanic centers in the Iskenderun Gulf area (Alici et al., 2001; Arger et al., 2000; Çapan et al., 1987; Rojay et al., 2001; Yurtmen et al., 2002). Geochemically, the volcanic rocks show predominantly mildly sodic,  $SiO_2$ -undersaturated compositions (Bilgin & Ercan, 1981; Yurtmen et al., 2000).

## 2.3. Karacadağ

The Karacadağ volcanic complex is located in southeastern Anatolia and comprises several volcanic fields distributed along the northern edge of the Arabian continent, in close proximity to the Anatolian orogen to the north (Figure 1; Allen et al., 2004). Mt. Karacadağ is the most prominent feature of the complex, forming a large elongate shield volcano over an area of approximately 10,000 km<sup>2</sup> (Lustrino et al., 2010). Magmatism commenced with the production of Siverek-phase plateau basalts during the middle–late Miocene to late Pliocene (~11.1–2.7 Ma; Ercan et al., 1990; Lustrino et al., 2010, 2012), possibly extending back to the early Miocene (Ekici et al., 2014). The initiation of Siverek volcanism during the Miocene correlates approximately with the onset of collision-related volcanism on the Erzurum-Kars Plateau in the north (Keskin, 2003; Keskin et al., 1998; Lustrino et al., 2010) and the broader uplift of the Anatolian Plateau.

More widely known, and sampled in the present study, are the volcanic products of late Miocene to Quaternary age (e.g., Ekici et al., 2014; Ercan et al., 1990; Lustrino et al., 2010, 2012; Pearce et al., 1990; Şen et al., 2004). This younger volcanic activity is divided into two distinct stages on the basis of stratigraphic and geochronological studies. The alkali basaltic and basaltic lava flows of the Karacadağ stage (1.9–0.8 Ma; Ercan et al., 1991; Pearce et al., 1990)—not to be confused with the volcanic complex of the same name—formed the main edifice of the volcanic complex, shortly after rapid uplift of the southeastern Anatolian Plateau (Faccenna et al., 2006; Keskin, 2003, 2007). This stage is inferred to be related to postcollisional rifting within the Arabian plate (Koçbulut et al., 2013). The young alkali basalts of the Ovabağ stage (0.4–0.1 Ma) represent a final minor phase of igneous activity on the (south) eastern side of the main edifice (Ekici et al., 2014; Ercan et al., 1991; Notsu et al., 1995). We collected four Quaternary basalts of the Ovabağ stage (Figure 1).

### 3. Methods

Whole-rock compositions of the studied samples were obtained by X-ray fluorescence spectrometry (major elements) and inductively coupled plasma mass spectrometry (ICP-MS; trace elements) using a Philips PW1404/10 and Thermo Electron X-series II ICP-MS, respectively, at the Vrije Universiteit Amsterdam, following standard procedures.

The selected rock samples were crushed and sieved to separate the olivine phenocrysts, after which they were mounted into epoxy holders and polished on one side to determine the compositions by electron microprobe analysis (EPMA; major elements). The most forsteritic olivine grains containing observable MI were selected to determine compositions and crystallization conditions of the parental melts through experimental and analytical work. The MI were rehomogenized and quenched experimentally using a high-temperature heating/quenching stage at the Vrije Universiteit Amsterdam following procedures outlined in Nikogosian et al. (2002). Afterward, the host-olivine grains were mounted in epoxy and polished until the MI were exposed at the surface for major, trace, and volatile element analysis by EPMA and laser ablation (LA)-ICP-MS.

EPMA data were obtained using a JEOL JXA-8530F field emission electron probe microanalyzer at Utrecht University, operated in wavelength dispersive mode, principally following the procedure described in de Hoog et al. (2001). Glass standards, natural and synthetic oxides, and metals were used as calibration standards. The probe current was 10 nA, the operating voltage was 15 kV, and the beam diameters used were 5  $\mu\text{m}$  for host olivines, 4  $\mu\text{m}$  for MI, and 1  $\mu\text{m}$  for spinel inclusions.

Trace elements were measured using LA-ICP-MS, using a GeoLas 200Q Excimer laser ablation system (193-nm wavelength) coupled to a Thermo Finnigan Element 2 sector field ICP-MS instrument at Utrecht University, following the procedures of Mason et al. (2008). The laser was operated with a 20- to 60- $\mu\text{m}$  spot size, using a pulse fluence of 5–10  $\text{J}/\text{cm}^2$  and a repetition rate of 10 Hz. The MI were ablated for approximately 25–30 s, with background count rates measured prior to and after ablation. Quantitative concentrations were calculated using National Institute of Standards and Technology (NIST) Standard Reference Material (SRM) 610 as a calibration standard (Jochum et al., 2011), with calcium (determined by EPMA) as an internal standard. United States Geological Survey (USGS) reference glass BCR-2G was used as a secondary standard throughout the analysis.

### 4. Results

#### 4.1. Whole-Rock Geochemistry

Figure 2 shows the major element classification and primitive mantle-normalized incompatible trace element patterns of the studied samples (supporting information Table S1). Kula samples show typical  $\text{SiO}_2$  and alkali content compared to published data (Figure 2a) and bear strong resemblance to OIB-type compositions with elevated abundances for many incompatible elements, including high-field-strength elements (HFSE; Nb, Ta, U, and Th) and large-ion lithophile elements (LILE; Rb, Ba, and Sr; Figure 2b). Two different compositional groups can be distinguished in our whole-rock data, irrespective of relative age. The first includes samples KUL-2A, KUL-3, KUL-4, KUL-5, KUL-6 and KUL-8, whereas the second consists of KUL-1 and KUL-7. The distinction is based on pronounced differences in MgO, CaO, total alkali (at similar silica content) and Cr content, as well as several HFSE (Nb, Ta) and LILE, such as Rb, Ba, and Sr.

Ceyhan-Osmaniye samples display relatively low  $\text{SiO}_2$  content, paired with relatively high total alkali content (Figure 2a). Compared to ÜÇT basalts, TOP basanites have notably lower  $\text{SiO}_2$ ,  $\text{Al}_2\text{O}_3$ , and CaO and higher  $\text{TiO}_2$ , total FeO,  $\text{Na}_2\text{O}$ ,  $\text{K}_2\text{O}$ , and  $\text{P}_2\text{O}_5$ , as well as highly and moderately incompatible trace element content. Primitive mantle-normalized incompatible trace element patterns (Figure 2c) of TOP rocks resemble OIB compositions, albeit with positive Nb, Ta, Sr, and P and negative Hf anomalies. ÜÇT patterns form shapes with generally similar interelemental fractionation, but display consistently lower abundances for most incompatible elements.

Karacadağ samples show a narrow range in  $\text{SiO}_2$  and total alkali content (Figure 2a), as well as in many other major oxide and trace elements. Primitive mantle-normalized incompatible trace element patterns (Figure 2d) approach typical OIB compositions and show slight differences in overall abundances, with variable positive anomalies for Sr, Nb, Ta, and Cs.

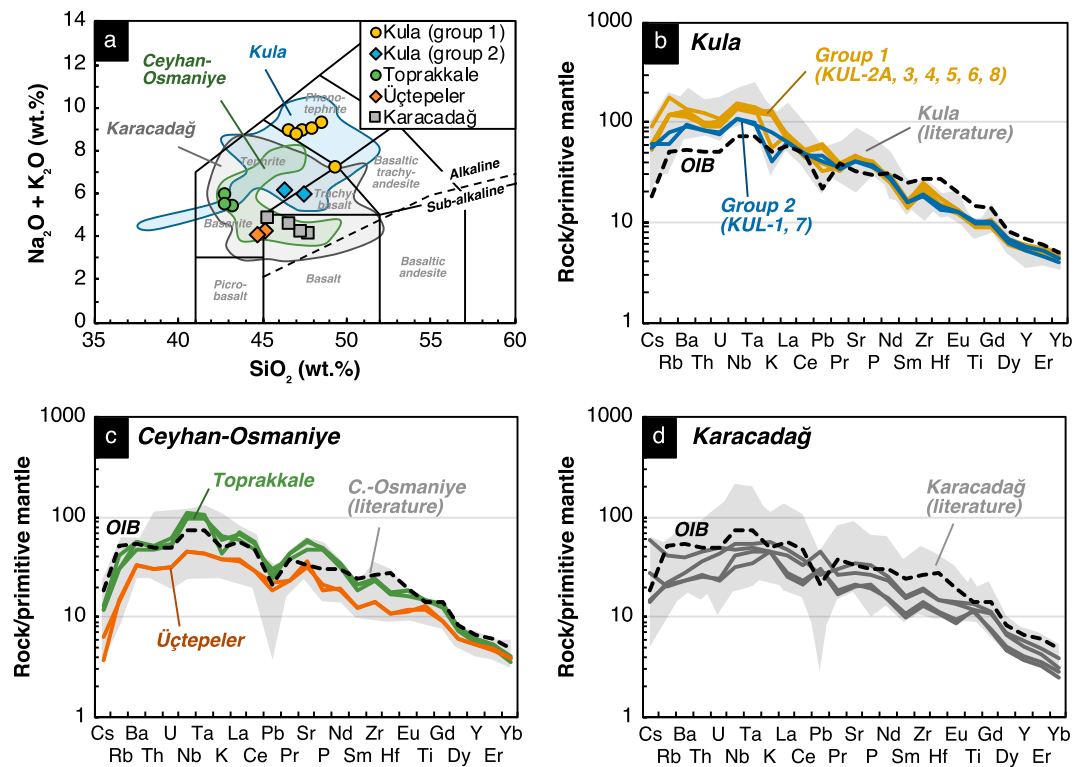


**Figure 2.** Classification diagrams for the studied whole-rock samples from Kula, Ceyhan-Osmaniye (Toprakkale and Üçtepeler), and Karacadağ. (a) SiO<sub>2</sub> versus total alkali (Na<sub>2</sub>O + K<sub>2</sub>O) classification diagram (Le Bas et al., 1986). Boundary between alkaline and subalkaline fields after Miyashiro (1978). Primitive mantle-normalized (McDonough & Sun, 1995) incompatible trace element diagram for (b) Kula, (c) Ceyhan-Osmaniye, and (d) Karacadağ lavas. Ocean island basalt (OIB) patterns (McDonough & Sun, 1995) and fields for literature whole-rock data (MgO ≥ 4 wt%) are shown for comparison. Data sources: Kula: Aldanmaz (2002); Aldanmaz et al. (2015); Alici et al. (2002)\*; Chakrabarti et al. (2012); Dilek and Altunkaynak (2010); Dyer (1987); Grützner et al. (2013)\*; Güleç (1991); Notsu et al. (1995); Sölpüker (2007)\*. Ceyhan-Osmaniye: Arger et al. (2000); Bağcı et al. (2011); Italiano et al. (2017); Yurtmen et al. (2000). Karacadağ: Ekici et al. (2012, 2014)\*; Lustrino et al. (2012)\*; Notsu et al. (1995); Pearce et al. (1990); Şen et al. (2004). Asterisks (\*) denote data sets for Kula and Karacadağ in which corresponding volcanic stages were reported.

## 4.2. Mineralogy

### 4.2.1. Olivine

Olivine phenocrysts in Anatolian samples (supporting information Table S2) display notable compositional diversity within the studied volcanic centers, even at similar forsterite content, as illustrated in Figures 3a–3c.

Kula samples carry two olivine populations (at Fo<sub>88–81</sub>), hereafter referred to as Group 1 (samples KUL-2A, KUL-3, KUL-4, KUL-5, KUL-6, and KUL-8), which show low CaO (~0.11–0.30 wt%, average ~0.2 wt%), and Group 2 (samples KUL-1 and KUL-7), which are characterized by higher CaO content (~0.20–0.36 wt%, average ~0.3 wt%). These groups coincide with those of the whole rocks (Figure 2b) and are unrelated to volcanic stage. The variability in terms of CaO content between the olivine groups could reflect the diversity of melt compositions present in the magma system.

The olivine phenocrysts from the Ceyhan-Osmaniye area (Fo<sub>87–72</sub>) show wide compositional diversity at similar Fo content, as shown in the Fo–CaO diagram (Figure 3b). Two groups of olivines can be distinguished, based on their compositions. ÜÇT olivines (samples OSM-4 and OSM-5) are characterized by high CaO (mainly ~0.18–0.28 wt%, average 0.23 wt%), which tends to increase with decreasing Fo, and relatively low NiO content (Figure 3b). Conversely, TOP olivines (samples OSM-1, OSM-2, and OSM-3) are marked by reaching notably lower CaO (~0.03–0.25 wt%, average 0.12 wt%), as well as slightly higher NiO content at given Fo content. The observed compositional diversity at high Fo cannot be reconciled with fractionation and could instead reflect the variability in primary melts.

The Karacadağ olivines (Fo<sub>85–74</sub>) are marked by a steep overall increase in CaO and decrease in NiO content with decreasing Fo (Figure 3c). The majority of the olivines plot close together, with relatively restricted ranges in CaO (0.1–0.3 wt%) and NiO (0.1–0.4 wt%).

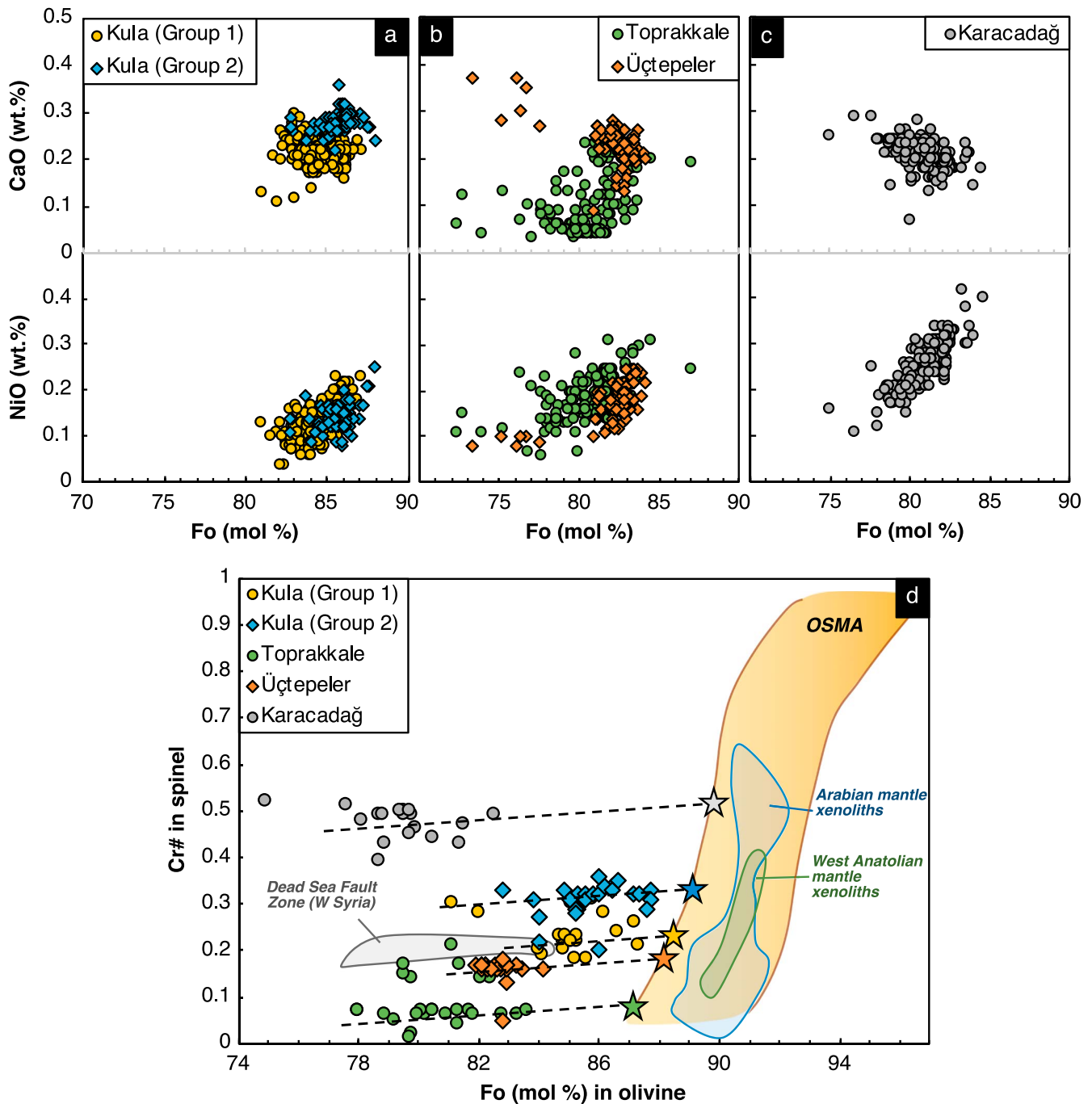


**Figure 3.** Forsterite (Fo) versus CaO and NiO content of olivine phenocrysts in the studied rock samples from (a) Kula, (b) Ceyhan-Osmaniye (Üçtepeler and Toprakkale) and (c) Karacadağ. (d) Relationships between Fo content of host olivine and Cr# [Cr/(Cr + Al)] of their spinel inclusions. OSMA = olivine-spinel mantle array for spinel peridotites (Arai, 1994). For comparison, fields of olivine-spinel pairs are shown for western Anatolian mantle xenoliths (Aldanmaz et al., 2005), Arabian mantle xenoliths (Stern & Johnson, 2010), and Syrian Dead Sea Fault Zone basalts (Al Ghab-Homs volcanic field; Ma et al., 2011). Dashed lines are compositional regression trends of associated olivine and spinel. Stars represent extrapolated (minimum) Fo content of the olivine groups in equilibrium with the mantle.

#### 4.2.2. Spinel

Spinel, occurring as inclusions in all types of olivine phenocrysts, show widely varying Cr numbers [Cr# = Cr/(Cr + Al)] and compositions (supporting information Table S3).

In Kula rocks, the olivine-hosted spinels corroborate the existence of two distinct compositional populations, which are linked to their host olivine groups (Figure 3a). The olivine-spinel pairs form two subhorizontal fractionation trends that approach the olivine-spinel mantle array (OSMA; Arai, 1994; Figure 3d). Spinel from (low-CaO) Group 1 olivines differ from spinels in (high-CaO) Group 2 by generally lower Cr# (0.16–0.32, average 0.24, and 0.20–0.36, average 0.30, respectively) at similar Mg# ranges (0.60–0.75). The Fo and Cr# of the olivine-spinel pairs of Group 1 suggest derivation from a slightly more fertile mantle source than those of Group 2.

In Ceyhan-Osmaniye, two spinel groups can be observed, again linked to their host olivine groups. ÜÇT spinels, enclosed by high-CaO host olivines, have high Cr# (~0.16; Figure 3d) and TiO<sub>2</sub> content (0.6–1.3 wt%). TOP spinels, which correspond to low-CaO olivines, are characterized by distinctly lower Cr# (~0.06; Figure 3d) and generally lower, though wider ranging, TiO<sub>2</sub> content (0.1–1.5 wt%). Similar to the olivine groups, TOP spinels show minor overlap with ÜÇT.

Karacadağ spinel inclusions, which are enclosed by relatively evolved olivines (Fo<sub>83–75</sub>), are marked by significantly higher Cr# (0.39–0.52, average 0.47; Figure 3d) and TiO<sub>2</sub> content (2.4–4.6 wt%, average 3.7 wt%) than the other Anatolian volcanic centers. The Cr# of the Karacadağ olivine-spinel pairs imply derivation from a significantly more depleted mantle source than inferred for Ceyhan-Osmaniye and Kula.

### 4.3. Melt Inclusions

#### 4.3.1. Petrography, Homogenization and Fe-Loss Correction of MI

In all the studied rock samples, olivine phenocrysts hosting primary magmatic inclusions were identified. The studied MI were present mostly as isolated inclusions, with some in small groups, oriented along growth zones of the host olivine, and are thus interpreted to be of primary origin (e.g., Roedder, 1984). Typically, MI were subspherical in shape, with sizes ranging from 10 to 100 μm. Since all MI were partially or fully crystallized, high-temperature microthermometric heating/quenching experiments were carried out to rehomogenize the MI prior to analysis. Based on 250 runs (supporting information Figure S1), the homogenization temperatures range between 1090 and 1270 °C for inclusions within Kula olivines (Fo<sub>83–87.5</sub>), 1110 and 1285 °C for inclusions within Ceyhan-Osmaniye olivines (Fo<sub>76–87</sub>), and between 1140 and 1240 °C for inclusions within Karacadağ olivines (Fo<sub>75–84.5</sub>).

Some of the homogenized MI from Ceyhan-Osmaniye and Karacadağ display lower FeO content than that of the host lavas (supporting information Figure S2 and Table S4) and show a negative correlation with the Fo content of their host olivines (supporting information Text S2 and Figure S2). This is typical for the reequilibration of Fe between MI and their host olivine phenocrysts during slow cooling prior to eruption (cf. Danyushevsky et al., 2000, Danyushevsky, McNeill, et al., 2002)—a process termed “Fe loss.” To correct for this postentrapment modification of MI compositions, the method of Danyushevsky et al. (2000) was followed, assuming a uniform initial FeO content corresponding to the FeO content of the respective host rocks. Both measured MI compositions and those corrected for postentrapment Fe loss are given in supporting information Table S4. Except for Mg and Fe, the maximum difference between measured and corrected values was modest for all elements (supporting information Figure S3), so that effect on the overall geochemical trends and variability within the MI compositions was insignificant.

Furthermore, the calculated temperatures of equilibrium between the corrected MI compositions and their olivine hosts are remarkably close to those experimentally determined by homogenization (±20 °C; supporting information Figure S5), demonstrative of a reassuring self-consistency of our methods. All corrections and calculations were carried out using Petrolog3 software (Danyushevsky & Plechov, 2011) and appropriate models (Borisov & Shapkin, 1989; Danyushevsky, 2001; Danyushevsky & Sobolev, 1996; Danyushevsky et al., 2000; Ford et al., 1983; Maurel & Maurel, 1982), and are detailed in supporting information Text S2.

#### 4.3.2. Major and Trace Elements

##### 4.3.2.1. Kula

The compositions of 77 MI trapped in Kula olivines (Fo<sub>87–83</sub>) are shown in Figure 4 and reported in supporting information Table S4. The MI display substantial variability when compared with the compositions of the host rocks and whole-rock literature data (references as in Figure 2), with especially large ranges in SiO<sub>2</sub> (43.3–53.5 wt%; Figure 4a), CaO (4.6–17.7 wt%; Figure 4b), Al<sub>2</sub>O<sub>3</sub> (15.4–22.9 wt%), K<sub>2</sub>O (0.9–4.0 wt%), and TiO<sub>2</sub> content (0.6–3.9 wt%), generally exceeding those of the whole rocks. The rocks further show variable

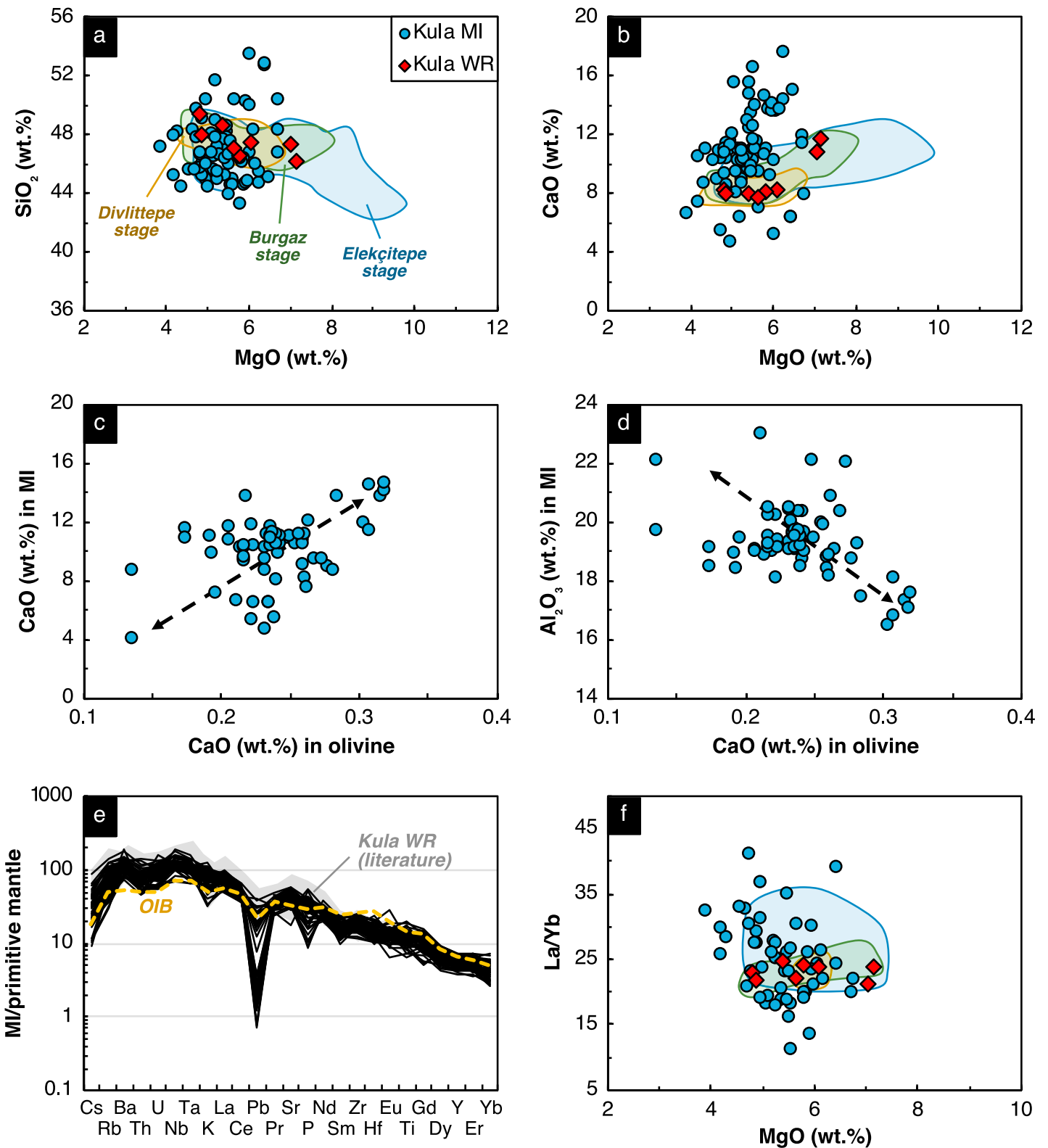


**Figure 4.** Variation diagrams for Kula melt inclusions (MI). MgO versus (a) SiO<sub>2</sub> and (b) CaO (wt%). CaO in host olivine versus (c) CaO and (d) Al<sub>2</sub>O<sub>3</sub> (wt%) in MI, illustrating correlations between major oxides in host olivine and MI. (e) Primitive mantle-normalized (McDonough & Sun, 1995) incompatible trace element diagram. (f) MgO (wt%) versus La/Yb in Kula MI. Host rocks, literature whole-rock (WR) fields (MgO ≥ 4 wt% and SiO<sub>2</sub> ≤ 50 wt%; references as in Figure 2), and ocean island basalt (OIB; Sun & McDonough, 1989) compositions are shown for comparison.

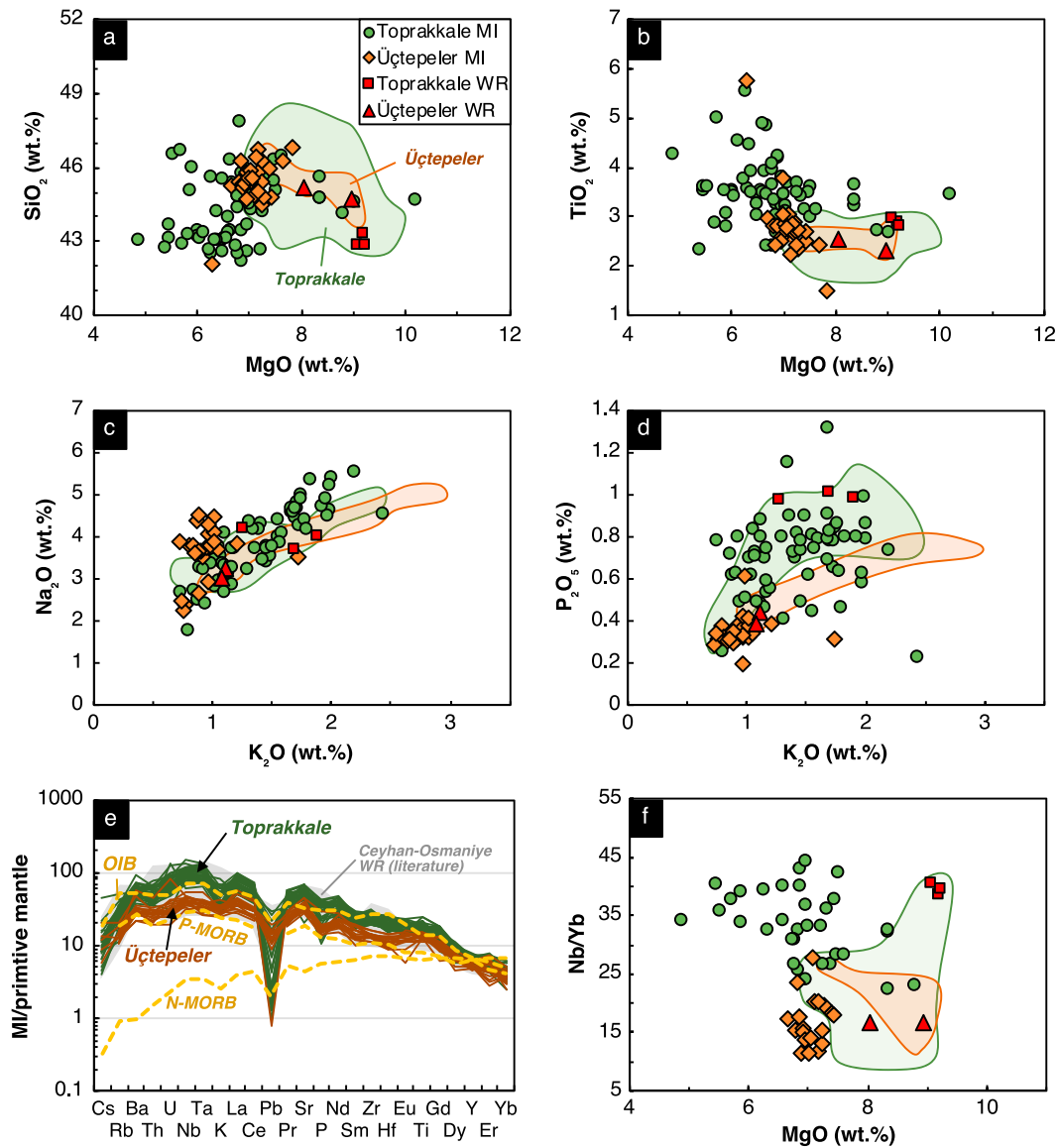


**Figure 5.** Variation diagrams for Ceyhan-Osmaniye melt inclusions (MI). MgO versus (a) SiO<sub>2</sub> and (b) CaO (wt.%). K<sub>2</sub>O versus (c) Na<sub>2</sub>O and (d) P<sub>2</sub>O<sub>5</sub> (wt.%), exemplifying the difference in major oxides in Üçtepeler and Toprakkale MI. (e) Primitive mantle-normalized (McDonough & Sun, 1995) incompatible trace element diagram. (f) MgO (wt%) versus Nb/Yb for Ceyhan-Osmaniye MI. Host rocks, literature whole-rock (WR) fields (MgO ≥ 6 wt% and SiO<sub>2</sub> ≤ 50 wt%; references as in Figure 2), plume mid-ocean ridge basalt (P-MORB; Saccani et al., 2013), ocean island basalt (OIB), and normal mid-ocean ridge basalt (N-MORB; Sun & McDonough, 1989) compositions shown are for comparison.

volatile content, for example, Cl (<100–2,528 ppm), F (<100–3,144 ppm), and S (<100–2,193 ppm). In the most forsteric olivines, the compositional diversity of trapped melts corresponds to mineral chemical grouping such that MI in (low-CaO) Group 1 olivines are characterized by lower CaO content (Figure 4c), as well as higher Al<sub>2</sub>O<sub>3</sub> (Figure 4d), SiO<sub>2</sub>, Na<sub>2</sub>O, K<sub>2</sub>O, P<sub>2</sub>O<sub>5</sub>, and Cl content, than those in (high-CaO) Group 2 olivines.

In general, Kula MI display enrichments in incompatible elements, with high LILE, light rare earth elements (LREE), and Nb-Ta abundances and relatively low LILE/HFSE values (e.g., Ba/Nb = 7–14). Their primitive mantle-normalized incompatible trace element patterns (Figure 4e) resemble those of the bulk lavas, approaching OIB-type trends, albeit with considerable enrichments in both LILE (e.g., Rb, Ba, and Sr) and HFSE (Nb, Ta, Th, and U) and with lower Pb minima. Furthermore, Kula MI lack negative Nb-Ta anomalies, indicating an absence of imprints from subduction-related components. Trace element variability in the MI at

given high MgO values (and host olivine Fo content), such as Ba (494–1,230 ppm), Sr (363–1,189 ppm), La (31–64 ppm), and Zr (126–261 ppm), is generally of similar order to that in compiled literature whole-rock data (references as in Figure 2). Similarly large ranges mark trace element ratios such as La/Yb (11–41; Figure 4f), Nb/Yb (22–96), and Zr/Y (6–13).

#### 4.3.2.2. Ceyhan-Osmaniye

The compositions of 88 MI trapped in Ceyhan-Osmaniye olivines ( $Fo_{87-77}$ ) are shown in Figure 5 and listed in supporting information Table S4. In the MgO versus major oxides diagrams (Figures 5a–5d), the large variability in melt compositions is apparent for virtually all major oxides, with considerable ranges in  $SiO_2$  (42.1–47.9 wt%),  $TiO_2$  (1.5–5.8 wt%),  $Al_2O_3$  (13.9–20.3 wt%), CaO (6.2–14.7 wt%),  $Na_2O$  (1.7–5.5 wt%),  $K_2O$  (0.7–2.4 wt%), and  $P_2O_5$  (0.2–1.3 wt%). Most notably, CaO and  $TiO_2$  content appears to reach significantly higher values than recorded in bulk lavas (references as in Figure 2), in contrast to  $SiO_2$ , which tends to reach lower values. The volatile content, F (<100–2,268 ppm), Cl (<100–1,072 ppm), and S (<100–4,006 ppm), is also variable. Overall, this diversity, present at restricted MgO intervals, cannot be reconciled with simple fractionation processes.

Again, clear compositional differences between the ÜÇT and TOP MI are discernible. ÜÇT MI collectively show high  $SiO_2$  content (44.5–46.8 wt%; Figure 5a) and low  $K_2O/TiO_2$  (0.2–0.4),  $TiO_2$  (1.5–3.0 wt%; Figure 5b),  $K_2O$  (0.7–1.2 wt%; Figure 5c),  $P_2O_5$  (0.2–0.4 wt%; Figure 5d), and Cl content (157–505 ppm; see also supporting information Figure S10), indicating a relatively narrow compositional range. Toprakale MI compositions show some overlap with ÜÇT MI but cover a notably wider range, including a distinct population characterized by lower  $SiO_2$  content (42.2–44.0 wt%) and higher  $K_2O/TiO_2$  (0.4–0.7),  $TiO_2$  (3.0–5.5 wt%),  $K_2O$  (1.4–2.4 wt%),  $P_2O_5$  (0.5–1.3 wt%), and Cl content (126–1,072 ppm). Similar to systematics observed in olivine and spinel, TOP MI also include compositions resembling ÜÇT MI, suggesting near-source mixing of compositionally different melts (see section 5.1.2).

Both groups show relative enrichments in many incompatible trace elements, including HFSE, LILE, and LREE over medium rare earth elements (MREE) and heavy rare earth elements (HREE). On the whole, they are marked by relatively low LILE/HFSE values (e.g., Ba/Nb = 4–8), positive anomalies for Ba and Sr, and lower Pb minima. However, TOP MI are considerably more enriched, displaying bell-shaped, OIB-like primitive mantle-normalized incompatible trace element patterns (Figure 5e) with slightly positive Nb-Ta anomalies, whereas ÜÇT MI patterns are flatter, characterized by lower abundances for most incompatible elements, including LREE, LILE, and HFSE, and a less pronounced positive Ba spike, as well as absent Nb-Ta anomalies. Their differences, at similarly high MgO content and host olivine Fo, are further visible in various trace element ratios, illustrating generally higher Nb/Yb (22–44 versus 12–28, respectively; Figure 5f) and LREE/HREE ratios (e.g., La/Yb = 18–33 versus 11–21) and lower LILE/HFSE (e.g., Ba/Nb = 3.9–7.2 versus 6.7–8.5) and HFSE/HFSE ratios (e.g., Zr/Ta = 57–89 versus 90–151).

#### 4.3.2.3. Karacadağ

The compositions of 82 MI trapped in Ovabağ-stage Karacadağ olivines ( $Fo_{85-75}$ ) are shown in Figure 6 and reported in supporting information Table S4. Major oxide diagrams (Figures 6a–6d) display the diversity in MI compositions. For many major oxides, such as  $TiO_2$ ,  $Al_2O_3$ , and  $P_2O_5$ , the compositional ranges are comparable to those of available whole-rock data (references as in Figure 2). However, the CaO (8.0–14.6 wt%) and  $Na_2O$  content (1.0–4.5 wt%) of the MI exceeds those of the bulk lavas. The volatile content, including F (<100–2,213 ppm), Cl (<100–736 ppm), and S (<100–2,276 ppm), is variable. Overall, the compositional variability represented by the MI at restricted MgO intervals cannot be the result of simple fractionation processes. Figures 6c and 6d illustrate the presence of a continuous array of MI compositions, in which CaO,  $SiO_2$ ,  $Na_2O$ ,  $K_2O$ ,  $P_2O_5$ , and Cl content and  $K_2O/TiO_2$  are correlated (see also supporting information Figure S11). These observations, given no correlation with Fo content of the host olivine, suggest the presence of at least two compositional end-members in the magma system—the mixture of which could account for the observed compositional spectrum. The first apparent end-member is characterized by notably higher  $K_2O$ ,  $Na_2O$ ,  $P_2O_5$ , Cl, and  $K_2O/TiO_2$  and lower CaO and  $SiO_2$  content than the second end-member.

Collectively, the MI show enrichments in the most incompatible elements, relatively low LILE/HFSE values (e.g., Ba/Nb = 4–10). Their primitive mantle-normalized incompatible trace element patterns (Figure 6e) are comparable to those of the whole rocks and resemble typical OIB-type patterns, though slightly less elevated for most LREE and MREE. The incompatible trace element patterns vary considerably in elevation, further

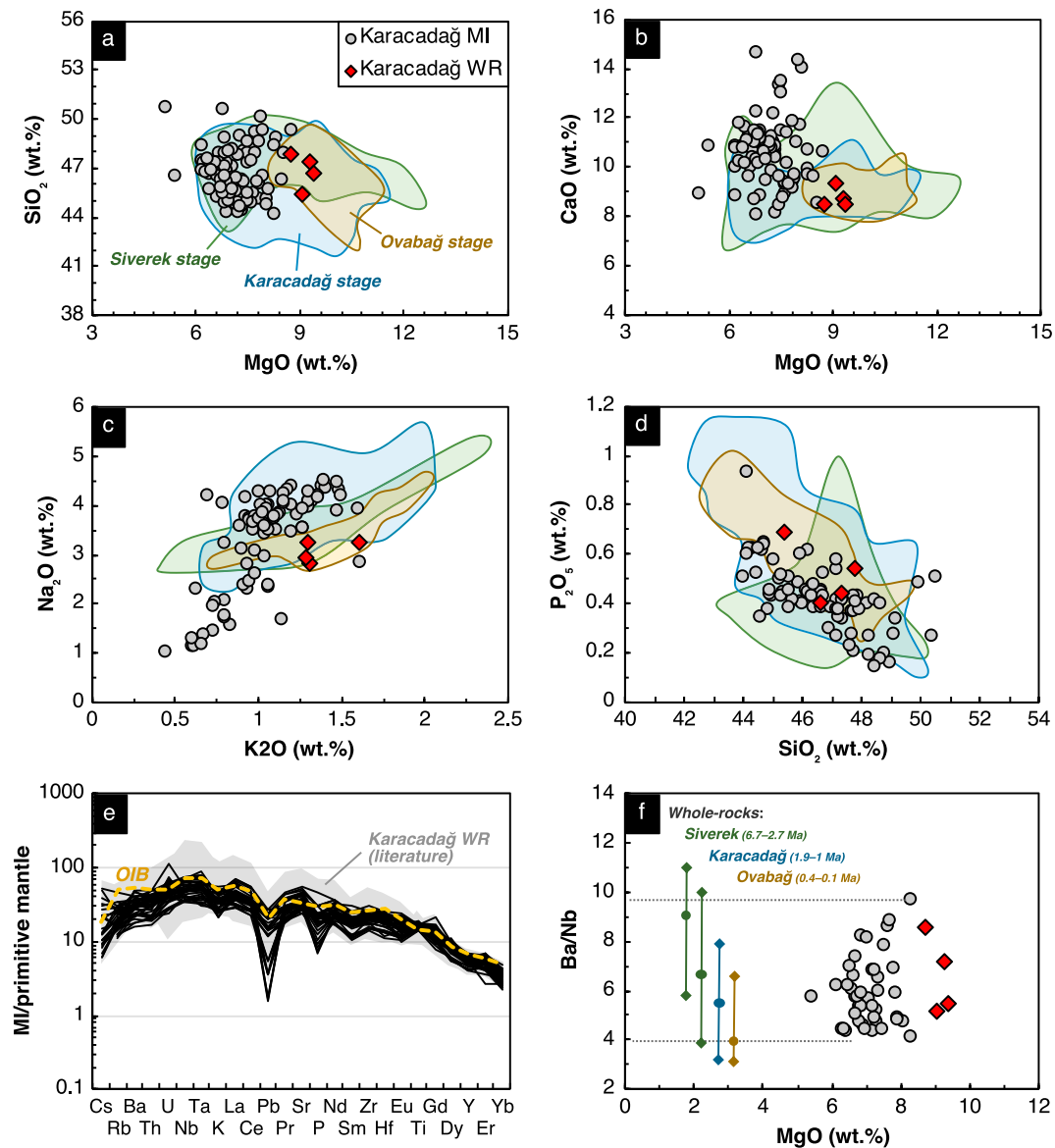


**Figure 6.** Variation diagrams for Karacadağ (Ovabağ stage) melt inclusions (MI). MgO versus (a) SiO<sub>2</sub> and (b) CaO, (c) K<sub>2</sub>O versus Na<sub>2</sub>O, and (d) SiO<sub>2</sub> versus P<sub>2</sub>O<sub>5</sub> (wt.%). (e) Primitive mantle-normalized (McDonough & Sun, 1995) incompatible trace element diagram. (f) MgO (wt%) versus Ba/Nb in Ovabağ-stage (0.4–0.1 Ma) Karacadağ MI, illustrating compositional diversity similar to the combined volcanic stages (6.7–0.1 Ma) represented by whole rocks (WR; Lustrino et al., 2012). Host rocks, literature WR fields (MgO ≥ 6 wt% and SiO<sub>2</sub> ≤ 50 wt%; references as in Figure 2) and ocean island basalt (OIB; Sun & McDonough, 1989) compositions are shown for comparison.

illustrating substantial compositional variability. Remarkably, trace element ratios in the MI, hosted exclusively by Ovabağ-stage (0.4–0.1 Ma) samples, cover virtually the entire compositional range recorded by the whole rocks, including earlier Siverek-stage (6.7–2.7 Ma) and Karacadağ-stage (1.9–0.8 Ma) rocks. This is of particular significance since whole-rock Ovabağ-stage data (e.g., Lustrino et al., 2012) seem to show a more restricted compositional range. Various trace element ratios, including Ba/Nb (4–10; Figure 6f), La/Nb (0.7–1.3) and Ti/Nb (395–898) testify that the melt diversity trapped in lavas of the youngest stage is of comparable magnitude as the entire compositional range seen in the stages combined (cf., Lustrino et al., 2012).

#### 4.3.3. Crystallization Conditions

The calculated olivine-MI equilibrium temperatures (supporting information Text S2 and Table S4), that is, entrapment temperatures, correlate well with Fo of the olivine phenocrysts and MgO content of the MI for

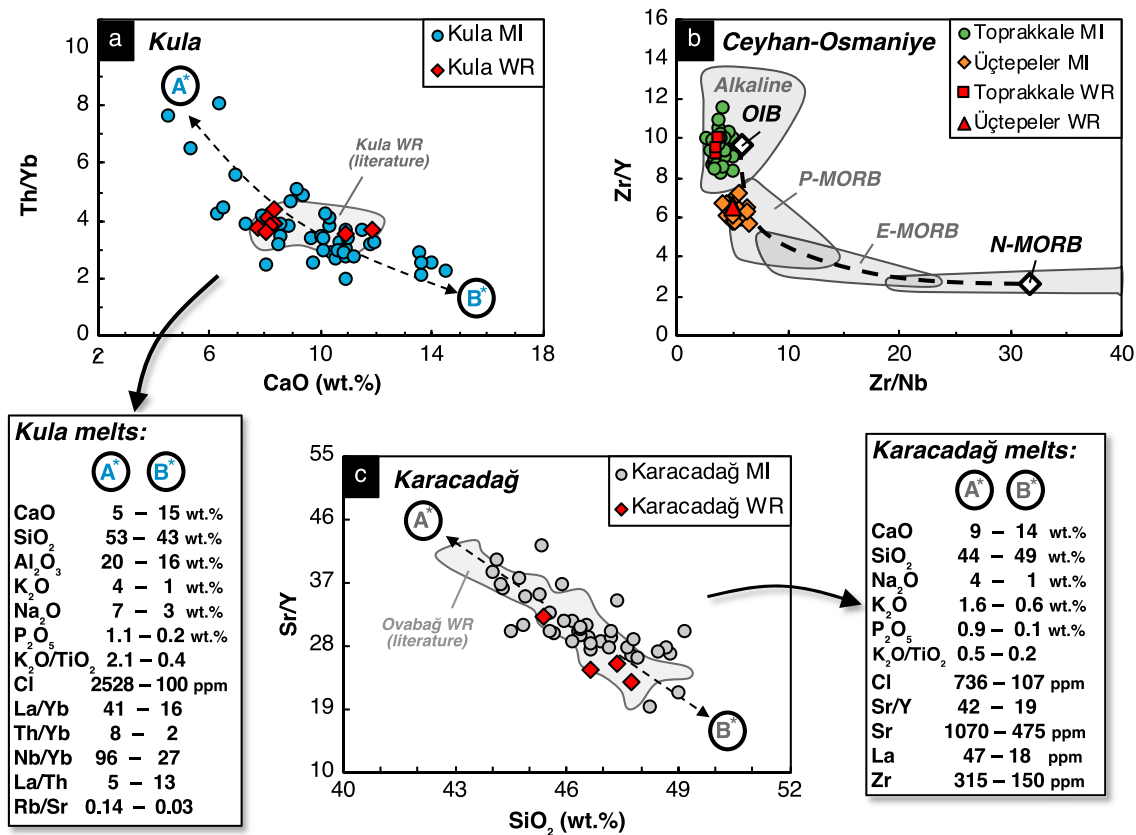


**Figure 7.** (a) CaO (wt.%) versus Th/Yb in Kula melt inclusions (MI), illustrating correlations between major oxides and trace element ratios. (b) Zr/Nb versus Zr/Y in Ceyhan-Osmaniye MI. Fields represent typical normal mid-ocean ridge basalt (N-MORB), enriched mid-ocean ridge basalt (E-MORB), plume mid-ocean ridge basalt (P-MORB) and ocean Island basalt (OIB) compositions (Saccani et al., 2014, and references therein). Dashed line indicates mixing line between typical OIB and N-MORB compositions (Sun & McDonough, 1989). (c) SiO<sub>2</sub> (wt.%) versus Sr/Y content in Karacadağ MI, illustrating correlations between major oxides and trace element ratios. Insets list major oxides and trace element ratios characteristic for each component. Asterisks (\*) denote end-member compositions in trapped melts, rather than calculated primary melts (discussed in section 5.3). Host rocks and literature whole-rock (WR) fields (references as in Figure 2) are shown for comparison. See text for discussion.

Ceyhan-Osmaniye and Karacadağ (supporting information Figure S4). Ranges of crystallization temperatures are 1280–1110 °C for olivines in Ceyhan-Osmaniye samples (Fo<sub>87–77</sub>) and 1255–1130 °C for olivines in Karacadağ samples (Fo<sub>85–75</sub>). Kula olivines show a large temperature range of 1275–1090 °C at narrow Fo (87–83 mol %) and MgO ranges. This pronounced variability in olivine-MI equilibrium temperatures corroborates the evidence for mixing of compositionally diverse melts, trapped in similarly high-Fo olivine phenocrysts (see section 5.1.1).

Calculated oxygen fugacity ( $fO_2$ ) values of the MI, expressed as <sup>10</sup>log units and plotted against crystallization temperatures in supporting information Figure S7, indicate oxidation states near the fayalite-magnetite-quartz (FMQ) and nickel-nickel oxide (NNO) redox buffers for all studied samples. Though largely similar, Kula ( $\Delta$ NNO ranging from –1.3 to 0.2) and Ceyhan-Osmaniye samples ( $\Delta$ NNO from –1.4 to 0.4) tend to reach somewhat lower oxidation states than Karacadağ samples ( $\Delta$ NNO from –0.9 to 0.5).

## 5. Discussion

### 5.1. Diversity of Parental Melts

The studied MI from Kula (Fo<sub>87–83</sub>), Ceyhan-Osmaniye (Fo<sub>87–77</sub>), and Karacadağ (Fo<sub>85–75</sub>) are hosted by olivines that contain somewhat lower forsterite content than those typically in equilibrium with mantle peridotite (Fo > 88; e.g., Arai, 1994). The following discussion includes only those melt compositions that were scrutinized to exclude any crystallizing phases on the liquidus other than olivine (detailed in

supporting information Text S3). These criteria ensure the exclusive (and reversible) effect of olivine crystallization on primary melt compositions, and because olivine does not include nor fractionate trace elements during crystallization, the diversity in trace element ratios of these MI has remained unchanged and represents that of the primary melts from which they have originated. We infer that these heterogeneous near-primary melts were entrapped during early olivine crystallization shortly after extraction from their mantle source. Hence, apparent end-member melt compositions enable us to identify mantle sources in considerably more detail than has been possible with primitive whole-rock compositions so far.

#### 5.1.1. Kula

Diversity in melt compositions defines two apparent end-member compositions (Figures 4c and 4d). A similar grouping is seen in primitive whole-rock, olivine, and spinel compositions. MI trapped in (low-CaO) Group 1 olivines are marked by low CaO content, as well as higher SiO<sub>2</sub>, Al<sub>2</sub>O<sub>3</sub>, Na<sub>2</sub>O, K<sub>2</sub>O, K<sub>2</sub>O/TiO<sub>2</sub>, P<sub>2</sub>O<sub>5</sub>, and Cl content, compared to those in (high-CaO) Group 2 olivines. At similar Fo content, they further show contrasting Cr# values for spinel inclusions (~0.2 and ~0.3, respectively; Figure 3d). In addition, Group 1 MI tend to be more enriched in incompatible trace elements than Group 2 MI, as shown by various ratios (e.g., Th/Yb; Figure 7a; La/Yb, Nb/Yb, and Rb/Sr; supporting information Figure S9). This compositional continuum suggests that the MI record mixing of two different mantle-derived melt components. Figure 7 a summarizes distinctive major and trace element characteristics of the low-CaO (~5 wt%) end-member component A\* and the high-CaO (~15 wt%) component B\* in the trapped melts.

In contrast to the compositional continuum of the MI, the olivine and spinel compositions tend to show more discrete populations (CaO<sub>ol</sub> ~0.3 and ~0.2 wt%; Cr#<sub>sp</sub> ~0.3 and ~0.2, respectively). These features can be attributed to early mingling of melts containing near-liquidus olivines and spinels, rapidly followed by MI entrapment during subsequent crystal growth when melts were still incompletely mixed. Such a scenario could also account for scatter in the MI compositions.

#### 5.1.2. Ceyhan-Osmaniye

Compositions of the most forsteritic olivines, spinel inclusions, and MI from the Ceyhan-Osmaniye area indicate the involvement of two chemically distinct types of parental melts in the generation of ÜÇT and TOP lavas. The observed compositional groups chiefly correspond to the melts that formed ÜÇT (samples OSM-4 and OSM-5) and TOP (samples OSM-1, OSM-2, and OSM-3) rocks. ÜÇT olivines are characterized by relatively high CaO and low NiO, whereas most TOP olivines are marked by notably lower CaO and higher NiO content (Figure 3b). This distinction is confirmed by spinel inclusions, which divide the populations with higher Cr# (~0.16) in ÜÇT, from lower Cr# (~0.06) in TOP (Figure 3d). The presence of high CaO olivines and some high Cr# spinels in TOP samples point to a near-source mixing/mingling scenario involving compositionally diverse melts, which ultimately gave rise to the composition of melts entrapped during early olivine crystallization.

The difference between ÜÇT and TOP melts is further represented by the compositional variability recorded in the MI (Figures 5a–5d and supporting information Figure S10). ÜÇT MI, though still exceeding whole-rock compositions, display a relatively narrow compositional range, with high SiO<sub>2</sub> and low K<sub>2</sub>O/TiO<sub>2</sub>, K<sub>2</sub>O, P<sub>2</sub>O<sub>5</sub>, TiO<sub>2</sub>, and Cl content. Conversely, TOP MI cover a considerably wider range and contain a distinct population characterized by lower SiO<sub>2</sub> and higher K<sub>2</sub>O/TiO<sub>2</sub>, K<sub>2</sub>O, P<sub>2</sub>O<sub>5</sub>, TiO<sub>2</sub>, and Cl content. Again, TOP MI include compositions resembling those of ÜÇT, in agreement with mixing relationships between the two populations in the early stages of magmatic evolution. Furthermore, in accordance with their whole-rock compositions, trace elements show that TOP MI are considerably more enriched and display OIB-like incompatible trace element patterns, whereas ÜÇT MI have lower abundances for most incompatible elements. To explore their relation further, Figure 7b illustrates that the Zr/Nb and Zr/Y ratios of ÜÇT MI plot remarkably close to the mixing line between typical normal mid-ocean ridge basalt (N-MORB) and OIB compositions (Sun & McDonough, 1989), showing highly enriched MORB (“plume mid-ocean ridge basalt (P-MORB)-like”) compositions (e.g., Gorryng et al., 2003; McKenzie & Bickle, 1988; Saccani et al., 2013, 2014). Indeed, the similarity between ÜÇT MI and enriched, P-MORB-like compositions is evident for many incompatible trace elements (Figure 5e), the significance of which will be discussed in the next section.

#### 5.1.3. Karacadağ

The diversity of primitive melt compositions in the studied Ovabağ-stage samples (0.4–0.1 Ma) essentially covers the entire compositional range as recorded by whole-rock data for all volcanic stages, including

Siverek (6.7–2.7 Ma) and Karacadağ (1.9–1 Ma). As demonstrated by their variable major element content (Figures 6a–6d), which display no correlation with Fo content of host olivine, the compositional diversity of the melts cannot be the result of simple fractionation processes.

The presence of a continuous array of MI compositions, in which CaO, SiO<sub>2</sub>, K<sub>2</sub>O, Na<sub>2</sub>O, P<sub>2</sub>O<sub>5</sub>, and Cl content are correlated (Figures 6c and 6d and supporting information Figure S11), suggest the involvement of two different parental melt components derived from the mantle source region, rather than one homogeneous parental melt. This notion is further supported by trace element systematics, which show covariations in accordance with major element trends. Significant variability in Sr/Y (Figure 7c), Sr, La, and Zr abundances range from low (in MI with low K<sub>2</sub>O, Na<sub>2</sub>O, P<sub>2</sub>O<sub>5</sub>, and Cl and high CaO and SiO<sub>2</sub> content) to high (in MI with high K<sub>2</sub>O, Na<sub>2</sub>O, P<sub>2</sub>O<sub>5</sub>, and Cl and low CaO and SiO<sub>2</sub> content). These covariations are consistent with melt entrapment during a state of incomplete mixing of compositionally diverse mantle-derived parental melt components.

Figure 7c summarizes the distinctive characteristics of these inferred end-member components in the trapped melts (A\* and B\*). Melt component A\* is characterized by relatively low CaO and SiO<sub>2</sub> content; high alkalinity and K<sub>2</sub>O/TiO<sub>2</sub>, P<sub>2</sub>O<sub>5</sub>, and Cl content; and a more enriched trace element signature, as evidenced by, for example, high Sr/Y, Sr, La, and Zr content. Conversely, component B\* is marked by relatively high CaO and SiO<sub>2</sub> content; low alkalinity and K<sub>2</sub>O/TiO<sub>2</sub>, P<sub>2</sub>O<sub>5</sub>, and Cl content; and less pronounced trace element enrichments, as shown by, for example, lower Sr/Y, Sr, La, and Zr content.

## 5.2. Mantle Sources

### 5.2.1. Kula

Postcollisional volcanism in western Anatolia has been interpreted to be closely linked to slab breakoff, lithospheric delamination, and passive asthenospheric upwelling, as a result of regional compressional and subsequent extensional tectonics (Alici et al., 2002; Dilek & Altunkaynak, 2007). South of the Izmir-Ankara-Erzincan suture zone, volcanic sources are thought to reflect an early Miocene to Quaternary transition from a subduction-modified lithospheric mantle to the upwelling of OIB-like asthenospheric mantle (Agostini et al., 2007; Aldanmaz et al., 2006, 2015; Alici et al., 2001; Dilek & Altunkaynak, 2007; Grützner et al., 2013; Innocenti et al., 2005; Karaoğlu & Helvacı, 2014). The Kula volcanic province, directly overlying a vertical tear in the subducted African slab (Berk Biryol et al., 2011; Chakrabarti et al., 2012; Klaver et al., 2016; van Hinsbergen, Kaymakci, et al., 2010), hosts rocks that exhibit clear OIB-like asthenospheric mantle signatures (Alici et al., 2002; Chakrabarti et al., 2012; Grützner et al., 2013). In addition, some authors have inferred a more limited contribution of an enriched lithospheric mantle component to account for Sr-Nd-Pb isotopic compositions and enrichments in incompatible trace elements relative to OIB compositions (Alici et al., 2002; Cesur et al., 2016; Lustrino & Wilson, 2007; Seyitoğlu et al., 1997).

Despite the compositional diversity, the Kula MI plot unequivocally on the MORB-OIB array on a Th/Yb versus Nb/Yb diagram (Figure 8a), indicating that the mantle source has not been affected by subduction enrichment or source contamination and, instead, solely reflects within-plate enrichments. Based on whole-rock isotope data, Lustrino and Wilson (2007) suggested the mixing of HIMU (high- $\mu$ ) and EM-type sources. On the basis of our primitive Kula melt compositions, which provide a unique window through the assimilation–fractional crystallization (AFC) and mixing processes that inevitably compromise whole-rock data, and by employing incompatible trace element ratios that have been shown to differ significantly between the two OIB subgroups (cf., Willbold & Stracke, 2006), we observe remarkable affinity with EM-type sources for Rb/Nb, Ba/Nb (Figure 8d), Rb/Th, La/Th, Rb/La, Rb/Ba, and Rb/Sr ratios. Future isotopic studies on primitive MI could prove helpful in further elucidating the characteristics of this enriched mantle source.

Several authors have explored the influence of degree and depth of partial melting on the geochemical signature of Kula magmas. Trace element modeling has suggested generally low degrees (<10%) of partial melting (e.g., Aldanmaz, 2002; Chakrabarti et al., 2012; Sölpüker, 2007) at different possible melting depths, ranging from spinel peridotite (Aldanmaz, 2002), the transition zone between garnet and spinel peridotite (McKenzie & O'Nions, 1995), to both garnet and spinel peridotite sources (Alici et al., 2002). The La/Sm versus Sm/Yb diagram in Figure 8e illustrates a nonmodal batch melting model for spinel and garnet lherzolite (Aldanmaz et al., 2000, and references therein), in which Kula MI, similar to whole-rock compositions, reflect relatively low degrees (<2%) of partial melting of a source region between the spinel (~50%) and garnet (~50%) stability fields. These features alone cannot fully account for the systematic compositional

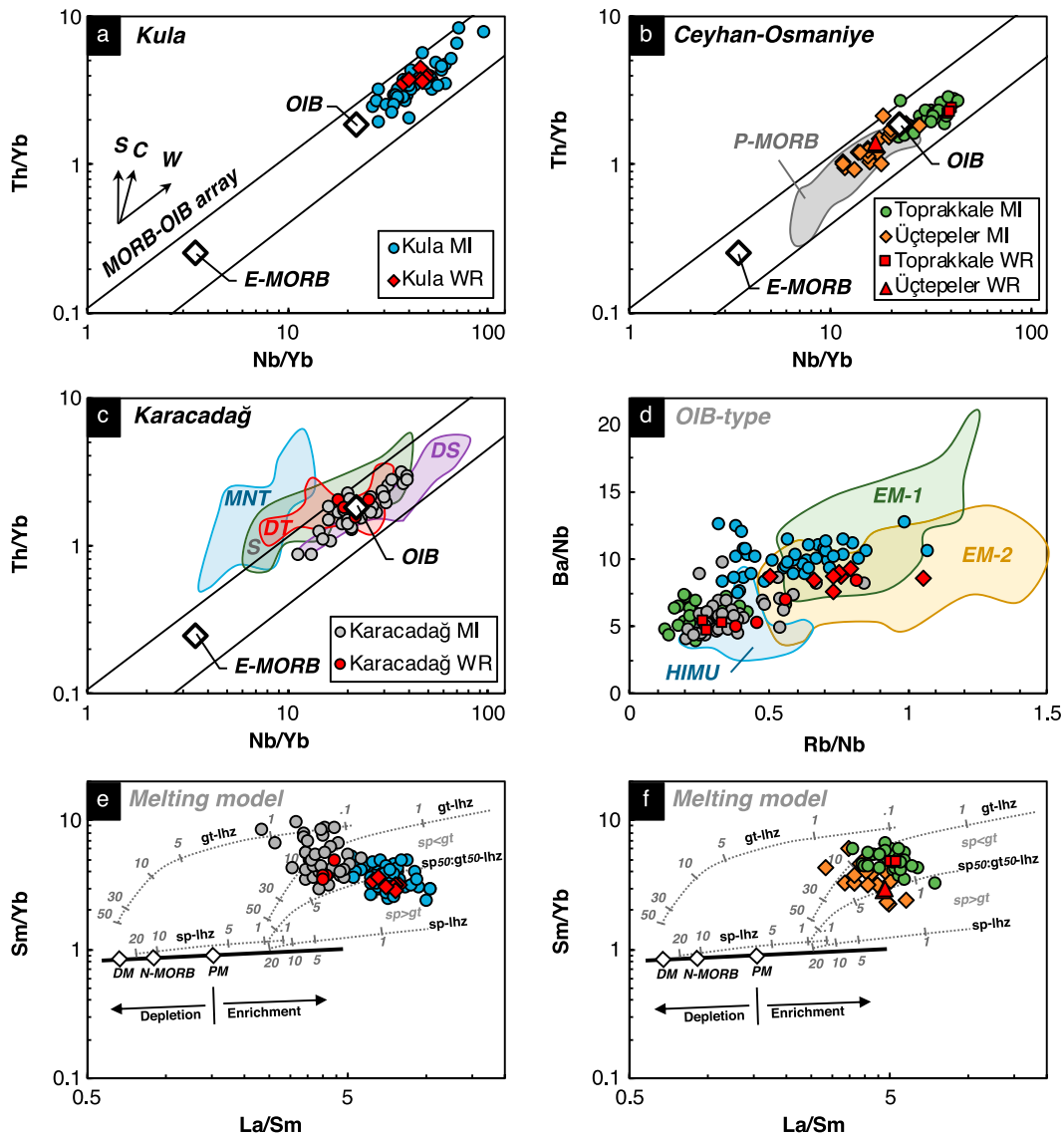


**Figure 8.** Nb/Yb versus Th/Yb in (a) Kula, (b) Ceyhan-Osmaniye, and (c) Karacadağ rocks. S = subduction zone enrichment trend; C = crustal contamination trend; W = within-plate enrichment trend (Pearce & Peate, 1995). (d) Rb/Nb versus Ba/Nb in ocean island basalt (OIB)-type melts from Kula, Ceyhan-Osmaniye, and Karacadağ, illustrating trace element characteristics of OIB subgroups (Willbold & Stracke, 2006). La/Sm versus Sm/Yb in (e) Kula, Karacadağ, and (f) Ceyhan-Osmaniye melt inclusions (MI), illustrating melt curves obtained using nonmodal batch melting (Aldanmaz et al., 2000, and references therein). Tick marks indicate percentage of partial melting. Heavy line represents mantle array. Lhz = lherzolite; gt = garnet; sp = spinel. Where relevant, compositions of primary mantle (PM), normal mid-ocean ridge basalt (N-MORB), enriched mid-ocean ridge basalt (E-MORB), and ocean island basalt (OIB; Sun & McDonough, 1989), depleted MORB mantle (DMM; McKenzie & O’Nions, 1991), HIMU, EM-1, and EM-2 (Willbold & Stracke, 2006, and references therein), typical P-MORB (Saccani et al., 2013, 2014), Muş-Nemrut-Tendürek (MNT) volcanics (Keskin, 2007, and references therein), Dead Sea Fault Zone volcanics (DT = SE Turkey (Alici et al., 2001; Italiano et al., 2017; Parlak et al., 1998)); DS = NW Syria (Ma et al., 2011) and NW Syrian (S) intraplate volcanics (Krienitz et al., 2006) are shown for comparison.

variability observed within the suite of primitive melts as evidenced by olivine-spinel-MI compositions. The heterogeneous nature of these phases suggests an initial state of incomplete mixing during the early stages of magma evolution, as supported by the large range of crystallization temperatures at narrow Fo content (87–83 mol %). The observed systematics, consistent with a near-source mixing scenario involving two different parental melt components, point to a chemically heterogeneous mantle source region. Indeed, for intraplate settings, multiple instances of extensive variability in primitive melt compositions have been interpreted in terms of a heterogeneous mantle sources (e.g., Rudge et al., 2013; Sobolev et al.,

2011, 2000; Stracke et al., 2003)—interpretations that have gained support from isotopic studies (e.g., Jackson & Hart, 2006; Maclennan, 2008; Saal et al., 1998; Sobolev et al., 2011).

### 5.2.2. Ceyhan-Osmaniye

Volcanic products in the İskenderun Gulf area have widely been recognized as originating from an OIB-like asthenosphere (Alici et al., 2001; Parlak et al., 2000, 1998, 1997; Polat et al., 1997; Yurtmen et al., 2000), in which magma ascent may have been facilitated by transtensional tectonics associated with the strike-slip fault systems bounding the African-Anatolian-Arabian plates since the late Pliocene (Bağcı et al., 2011; Italiano et al., 2017; Lustrino & Sharkov, 2006; Parlak et al., 2000; Polat et al., 1997). Additionally, several authors have noted that volcanics in this area, as well as in central Anatolia, exhibit geochemical signatures associated with subduction-related metasomatic processes (Bağcı et al., 2011; Italiano et al., 2017; Polat et al., 1997; Reid et al., 2017; Yurtmen et al., 2000).

However, a role for subduction-related fluids, to account for the variably enriched incompatible trace element content of Osmaniye area rocks (Italiano et al., 2017; Yurtmen et al., 2000), is inconsistent with the observed trace element systematics and, particularly, low LILE/HFSE for primitive melts in both ÜÇT and TOP (Figure 5e). Indeed, variations of elemental ratios for both ÜÇT and TOP, which plot within the mantle array (Figure 8b), argue against subduction zone enrichment and/or source contamination and, instead, reflect differences in terms of within-plate enrichments. TOP MI include typical OIB-like compositions, which are marked by, for example, low SiO<sub>2</sub> and high K<sub>2</sub>O/TiO<sub>2</sub>, K<sub>2</sub>O, TiO<sub>2</sub>, P<sub>2</sub>O<sub>5</sub>, Cl, and Nb/Yb, relative to ÜÇT (Figure 5 and supporting information Figure S10). While these compositions are typical for derivation from an asthenospheric mantle source, ÜÇT melts show highly enriched MORB (P-MORB-like) compositions (Figures 5e, 7b, and 8b). We interpret the coexistence of these primitive melts as the result of interaction between OIB-like asthenosphere and a MORB-type source, which has produced melts variably enriched in incompatible trace elements (Figure 5e). The wide range of compositions present in TOP MI, some of which approach those of ÜÇT, fit well with the inferred near-source mixing/mingling scenario in the mantle, wherein the variable interaction between the two has generated compositions ranging from OIB to P-MORB-like affinity.

This scenario is further substantiated by rare earth element models on the role of the degree of partial melting and spinel/garnet involvement. La/Sm and Sm/Yb ratios (Figure 8f) suggest that at similarly low (<10%) degrees of partial melting, TOP and ÜÇT melts have been derived from a source region between the spinel (0–50%) and garnet (50–100%) stability fields. This implies that the compositional variability in melt compositions cannot be reconciled with systematic differences in degree of partial melting. Moreover, in contrast to the EM-like mantle source beneath Kula, incompatible trace element ratios such as Rb/Nb, Ba/Nb (Figure 8d), Rb/Th, La/Th, Rb/La, Rb/Ba, and Rb/Sr indicate that the OIB-type, asthenosphere-derived melts in the Ceyhan-Osmaniye region bear strong resemblance to typical HIMU compositions.

### 5.2.3. Karacadağ

The magmatic source for Miocene–Quaternary volcanism in the Karacadağ Volcanic Complex has been identified as resembling predominantly OIB-like asthenosphere (Lustrino et al., 2012; Şen et al., 2004), though possibly metasomatized and compositionally heterogeneous, involving metasomatic networks in the local upper lithospheric mantle (Lustrino et al., 2012; Pearce et al., 1990). Isotope data further suggest a mantle source possibly distinct from that of magmatism attributed to the Afar plume (Ekici et al., 2012, 2014), although some authors have noted similarities (Faccenna et al., 2013; Keskin et al., 2012b).

The interplay between two different primitive melt components in the mantle source region (Figure 7c), as discussed in the previous section, cannot be reconciled with either subduction zone enrichment or source contamination, as all Karacadağ MI show Nb/Yb and Th/Yb ratios that lie on the mantle trend (Figure 8c). This also distinguishes Karacadağ mantle sources from other intraplate-type volcanics in southwestern Anatolia, such as Muş-Nemrut-Tendürek (e.g., Keskin, 2007; Pearce et al., 1990), which are displaced from the MORB-OIB array toward elevated Th/Yb values, indicating crustal assimilation and/or a small inherited subduction-type enrichment (Pearce et al., 1990), and to lower Nb/Yb, suggesting derivation from a less enriched source (and possibly the presence of residual garnet in the mantle source of Karacadağ). In terms of within-plate enrichments, Karacadağ MI plot closer to Arabian intraplate volcanics in northwestern Syrian (e.g., Krienitz et al., 2006), though these are marked by slight Th/Yb enrichments that could be attributed to crustal assimilation. Characteristic incompatible trace element ratios, such as Rb/Nb, Ba/Nb (Figure 8d), Rb/Th,

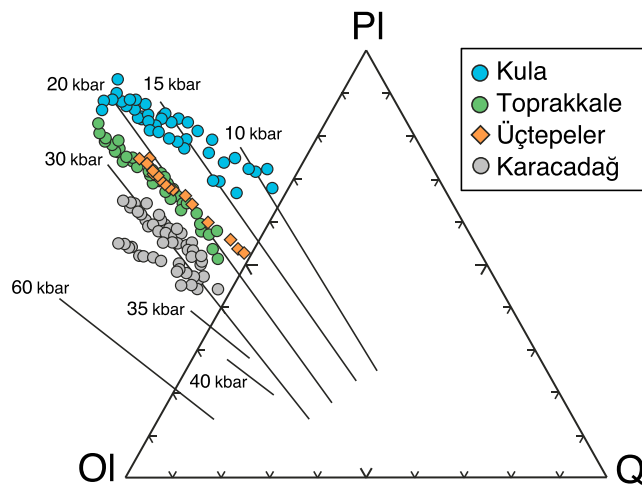


**Figure 9.** Estimates of primary melt generation pressures. Normative compositions of melts and the isobaric compositional trends in ternary projections (Walker et al., 1979). Projection from diopside onto the plane olivine-plagioclase-quartz (Ol-Pl-Q). Lines represent isobars of mantle magma compositions coexisting with the harzburgite-lherzolite assemblage, calculated on the basis of experimental data on the melting of mantle material (Falloon et al., 1988, and references therein; Hirose & Kushiro, 1993).

La/Th, Rb/La, Rb/Ba, and Rb/Sr, further indicate that the OIB-type asthenospheric mantle source beneath Karacadağ resembles typical HIMU compositions—a finding consistent with that of Lustrino et al. (2012).

To further investigate the occurrence of the two inferred parental melt components, we consider the role of partial melting and spinel/garnet involvement in the generation of compositional variability. Although constraints on the degree of partial melting of Karacadağ melts are scarce, recent rare earth element modeling by Ekici et al. (2014) has suggested mixtures of melts derived over a range of depths for Karacadağ- and Ovabağ-stage lavas, wherein mixtures of 1.5–5% partial melt of a phlogopite-bearing garnet and <1% partial melts from anhydrous lherzolite could account for most geochemical features of the whole rocks. Lustrino et al. (2012) have advocated the role of polybaric tapping diverse partial melts from a chemically and mineralogically heterogeneous shallow mantle source to explain the geochemical variations. Nonmodal batch melting models of garnet and spinel lherzolite for La/Sm and Sm/Yb (Figure 8e) suggest that the Ovabağ-stage MI represent relatively low degrees (<10%) of partial melting from depths between the spinel (0–50%) and garnet (50–100%) stability fields. Clearly, the compositional diversity in primitive melts, as recorded by primitive MI compositions, cannot be reconciled solely with a varying degree of partial melting. Similar to what we envision for Kula, the heterogeneous character seems to reflect the involvement and incomplete mixing of different parental melt components

early in the magmatic evolution. Despite the contribution of variations in degree of partial melting to the compositional diversity, the observed variability in primitive melts strongly suggests a heterogeneous mantle source. The heterogeneity postulated by Lustrino et al. (2012), who envisaged a temporal variation in major and trace elements in whole rocks as reflective of progressive exhaustion of a metasomatic network in the upper mantle, cannot fully account for the range in melt compositions recorded by our Ovabağ-stage MI (see section 5.1.3). Our MI demonstrate that despite temporal trends in whole-rock data, which might reflect mixing proportions, the heterogeneity of the Karacadağ mantle source is a feature that has persisted into the most recent stage of volcanic activity.

### 5.3. Primary Melts

#### 5.3.1. Conditions of Primary Melt Crystallization

The studied primitive magmatic inclusions further allow us to determine the conditions of primary melt crystallization. As illustrated in Figure 3d, the studied olivines hosting MI plot outside the mantle array and show scattered Fo ranges ( $Fo_{87-83}$  in Kula,  $Fo_{87-77}$  in Ceyhan-Osmaniye, and  $Fo_{85-75}$  in Karacadağ), implying that the melts have experienced variable amounts of olivine crystallization prior to entrapment. Using the primitive MI selected to exclude any other crystallizing phases on the liquidus except olivine (outlined in section 5.1), and assuming that the parental melts in the studied Anatolian volcanic centers were initially in equilibrium with typical mantle olivine, primary melt compositions were estimated by simulating reverse fractional olivine crystallization, using the model of Danyushevsky et al. (2000) (detailed in supporting information Text S3). The target Fo content used in this calculation was estimated from extrapolation of the relations between olivine Fo content and associated spinel Cr# in the different compositional groups onto the OSMA (illustrated by star symbols in Figure 3d), yielding a minimum value of Fo in equilibrium with the mantle. These values are  $Fo_{88.5}$  for Kula Group 1,  $Fo_{89}$  for Kula Group 2,  $Fo_{87}$  for TOP (OSM-1, OSM-2, and OSM-3),  $Fo_{88}$  for ÜÇT (OSM-4 and OSM-5), and  $Fo_{90}$  for Karacadağ (KAR-1, KAR-2, KAR-3, and KAR-4).

The calculated primary melt compositions (supporting information Table S4) are characterized by high MgO content for Kula (MgO = 8.9–6.5 wt%), TOP (MgO = 12.1–9.5 wt%), ÜÇT (MgO = 11.6–10.0 wt%), and Karacadağ (MgO = 16.1–13.4 wt%). Importantly, the systematic variability and groupings in trapped melt compositions, such as discussed in section 5.1, are similarly present in the calculated primary melts (supporting information Text S3), as these calculations have yielded only a minor shift in major oxide ranges, and did not affect trace element ratios.

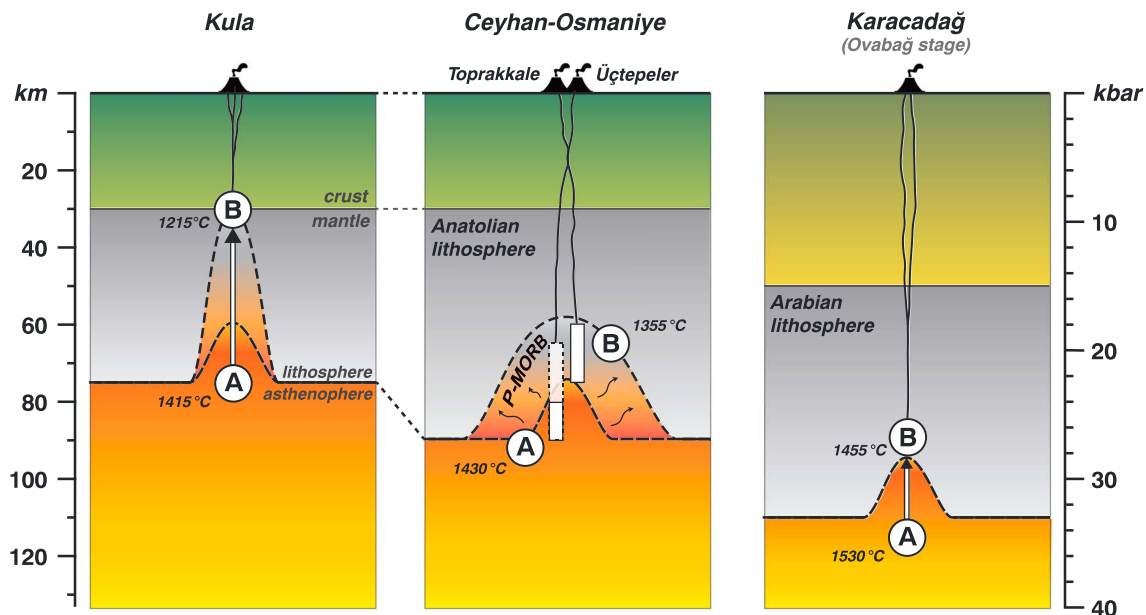


**Figure 10.** Schematic mantle models for the magma generation below Kula, Ceyhan-Osmaniye, and Karacadağ, indicating primary melt generation conditions and melt components A and B in each of the regions (section 5.3.2). Melting column below Toprakkale indicates ocean island basalt (OIB)-type (opaque white) and mixed-in plume mid-ocean ridge basalt (P-MORB)-like components (translucent white).

The temperature ranges obtained for the crystallization of the different primary magmas are 1340–1195 °C ( $F_{O_{89-88.5}}$ ) for Kula, 1335–1265 °C ( $F_{O_{87}}$ ) for TOP, 1310–1275 °C ( $F_{O_{88}}$ ) for ÜÇT, and 1405–1350 °C ( $F_{O_{90}}$ ) for Karacadağ.

Furthermore, estimated oxygen fugacities of primary melt crystallization (detailed in supporting information Text S4) correlate well with the observed compositional end-members in each volcanic district (supporting information Figure S7b). In all three areas, the deeper component (A) is marked by lower  $\Delta NNO$  (i.e., oxygen fugacity expressed as deviation from the NNO buffer in log units;  $-0.8$  to  $-0.5$ ) than that of component B ( $\Delta NNO \sim 0.2$  to  $0.4$ ).

### 5.3.2. Conditions of Primary Melt Generation

Experimental studies on partial melting of mantle material at various pressures allow the quantification of the dependence of magma composition, coexisting with an ultrabasic association, on pressure, temperature, and degree of melting (Sobolev & Nikogosian, 1994, and references therein). The sensitivity of the projection of a basalt tetrahedron on the olivine-plagioclase-quartz side to pressure enables quantitative estimation of the pressure of primary melt generation to within  $\pm 3$  kbar (in the range of 30–5 kbar), given that the melt composition is known and the assumption of a lherzolitic (harzburgitic) source is valid. The resulting pressures of primary melt generation (Figure 9) are 23–9 kbar for Kula, 28–19 kbar for TOP (28–25 kbar for the TOP OIB component), 23–18 kbar for ÜÇT (P-MORB-like component), and 35–27 kbar for Karacadağ (supporting information Table S4). Assuming a uniform geostatic gradient of 3.3 km/kbar, these values correspond to primary melt generation depths of 75–30 km for Kula, 90–65 km for TOP (90–80 km for the TOP OIB component), 75–60 km for ÜÇT (P-MORB-like component), and 115–90 km for Karacadağ (Figure 10).

When the effect of volatiles is negligible, the magma equilibrium temperature can be assumed to equal the calculated liquidus temperature. The calculation of the last equilibrium event between the primary melt and the mantle residue was based on the slope of the liquidus established for olivine-containing systems, corresponding to 5 °C/kbar (Takahashi & Kushiro, 1983). The pressure was then calculated from the adiabatic decompression of the primary melt with an adiabatic curve slope of 3 °C/kbar (Nisbet, 1982). The resulting primary melt formation temperatures are 1415–1215 °C for Kula, 1430–1350 °C for TOP (1430–1390 °C for the TOP OIB component), 1400–1355 °C for ÜÇT (P-MORB-like component), and 1530–1455 °C for Karacadağ (supporting information Table S4).

Compared to modeling work by Çoban (2007), who simulated primary mantle-equilibrated magmas with parameterized anhydrous and H<sub>2</sub>O-undersaturated experimental melts for Anatolian volcanics, our temperature estimates show reasonable agreement (mostly  $\pm 50$  °C). The calculated pressures of Çoban (2007) are considerably higher for Kula and Ceyhan-Osmaniye, which seem to reflect his consistent normalization to rather high MgO content (15 wt%) in these areas. Moreover, Reid et al. (2017) inferred melt equilibration conditions for Anatolian basalts. While their inferred mantle melting temperatures are either within (Kula and TOP) or close to our estimated temperature ranges (ÜÇT and Karacadağ), their pressure estimates differ more significantly, which could stem from their indirectly derived primary melt compositions and assumptions on the mantle-melt equilibrium forsterite content, which we have obtained directly from MI and olivine-spinel compositions.

Furthermore, our obtained temperature ranges for primary melt generation are of similar magnitude as those reported for regional volcanics in the wider Arabian and North African region, including Syria, the Dead Sea Fault region, Saudi Arabia, Yemen (Krienitz et al., 2009), Egypt (Abu El-Rus & Rooney, 2017), and the Afar plume (Beccaluva et al., 2009), which collectively range from  $\sim 1350$  to  $1550$  °C (supporting information Figure S8).

We further observe a clear correlation between our primary melt generation conditions (temperature, pressure, and depth) and the compositions of both the trapped and calculated primary melt end-members for each of the three volcanic districts (supporting information Figures S9f, S10d, and S11f). In the case of Kula and Karacadağ, melt component A represents the deepest levels of primary melt generation, whereas component B is located at shallower levels (Figure 10). Also, for Ceyhan-Osmaniye the OIB (A) and P-MORB-like (B) affinities are consistent with their deeper and shallower levels of primary melt generation, respectively (Figure 10). This further supports a petrogenetic model in which ascending asthenosphere and shallower, depleted (MORB-type) mantle have interacted in variable degrees below Ceyhan-Osmaniye to give rise to a compositional continuum, from OIB to P-MORB-like affinity.

#### 5.4. Origin of Recent Anatolian Intraplate Magmatism: Regional Plume or Local Geodynamics?

The quantification of the conditions of primary melt generation that we describe above reveals marked differences between the melt columns involved in intraplate-type magmatism across Anatolia. These reveal a first-order correlation with the depth of the lithosphere-asthenosphere boundary (LAB) at their current locations (Figure 10). The cause of varying thickness of the mantle lithosphere between the three study areas lies in tectonic processes. The greatest lithospheric depth, below Karacadağ ( $\sim 110$  km according to *S* wave receiver functions; Angus et al., 2006), represents the thickness of the essentially undeformed Arabian continental lithosphere. Ceyhan-Osmaniye lies above the southern part of the Anatolian fold-thrust belt, which consists of stacked crustal units scraped off from Gondwana-derived continental lithosphere (van Hinsbergen, Kaymakci, et al., 2010; van Hinsbergen et al., 2016). The original lithosphere was subducted to form the slabs below Anatolia, and the modern mantle lithosphere consequently regrew after crustal accretion and is hence younger and thinner than for the Arabian continent ( $\sim 90$  km according to *S* wave receiver functions; Kind et al., 2015). Finally, in western Turkey, below Kula, this accreted nappe sequence and young regrown lithospheric mantle was strongly extended in the Miocene (e.g., Bozkurt & Oberhänsli, 2001; Gessner et al., 2013) and is therefore the thinnest ( $\sim 75$  km; Kind et al., 2015).

Our new estimates for the origin of the intraplate volcanics reveal a first-order correlation with the depth to the LAB: Primary melts at Kula were generated at 75- to 30-km depth, at Ceyhan-Osmaniye at  $\sim 90$ – $65$  km, and at Karacadağ at  $\sim 115$ – $90$  km. This demonstrates in all three cases that melting likely occurred around the LAB (Figure 10). In all three areas, the rise of magma to the surface was likely facilitated by local deformation structures. The Menderes massif of western Turkey is cut by several major extensional detachment faults and associated cross-cutting graben-bounding normal faults, which appear to have allowed the rise of Kula melts (Alici et al., 2002; Innocenti et al., 2005). Ceyhan-Osmaniye melts rose to the surface along the major East Anatolian transform fault zone, and the Karacadağ melts may have used normal faults that formed in the Arabian foreland (Şengör & Yilmaz, 1981).

Finally, the three study areas share melts that do not appear to have been derived from mantle influenced by subduction. This observation can be readily reconciled with the modern geodynamic setting. No active subduction occurred below Karacadağ, which is located on the Arabian foreland; Ceyhan-Osmaniye is

located in a segment where the Bitlis slab, and probably also the eastern part of the Cyprus slab, broke off (Faccenna et al., 2006; Hafkenscheid et al., 2006; Portner et al., 2018). Below western Anatolia, in the area of Kula, the African slab has also detached and opened a slab gap (Berk Biryol et al., 2011; Bocchini et al., 2018; van Hinsbergen, Kaymakci, et al., 2010). Hence, in all three areas, primitive, OIB-like asthenosphere could have had access to the base of the lithosphere.

The Anatolian intraplate volcanics have a geochemical signature of a “normal” upper mantle. However, the upper mantle normally does not melt, unless it is heated, hydrated, or decompressed. The geochemistry of the Turkish intraplate volcanics exclude hydration. It is then tempting to first search for the causes of melting by decompression, related to the regional tectonic and geodynamic evolution of the Anatolia, assessing whether melting correlates with the formation of, for example, slab gaps or the occurrence of major extension that may have triggered regional mantle flow and decompression. Such correlations, however, are challenging to find, as we explain below.

For Kula, volcanism has been correlated with the extension of the Menderes massif (Alici et al., 2002; Innocenti et al., 2005) and the formation of a slab gap (Bocchini et al., 2018; Dilek & Altunkaynak, 2009). However, while both tectonic events unequivocally occurred, there seems to be no direct temporal correlation with the volcanism. The vast majority of extension in the Menderes massif occurred between 25 and 5 Ma, and extension rates had considerably dropped in western Turkey by 5 Ma (Bozkurt & Oberhänsli, 2001; Ring et al., 2003; van Hinsbergen, 2010). The extension in western Turkey accommodated a vertical axis rotation difference, and the amount of extension decreased eastward toward a pivot point located close to Kula (van Hinsbergen, Dekkers, et al., 2010). Volcanism in Kula thus occurred in the region of the Menderes massif least affected by extension, after the vast majority of extension had already been accommodated prior to volcanic activity. In addition, estimates for the timing of breakoff of the east Aegean slab below western Anatolia, forming the slab gap facilitating asthenospheric rise, suggest that it happened at least ~15 Ma (Faccenna et al., 2006; van Hinsbergen, Kaymakci, et al., 2010; Jolivet et al., 2015). The presence of a disconnection between the Aegean and Antalya and/or Cyprus slabs has been postulated to have already existed in late Oligocene–early Miocene times based on tectonic arguments (Gessner et al., 2013), as well as the geochemistry of lower Miocene volcanics in the eastern Aegean region (Klaver et al., 2016). A first-order difference in rollback concluded from the ages of central Anatolian and Aegean back-arc extension may even suggest that the Aegean and central Anatolian slabs were decoupled since the Late Cretaceous, potentially by torroidal mantle flow ever since that time (Gürer et al., 2018). While the deformation structures and the slab gap of western Anatolia are undoubtedly important boundary conditions in the formation of the Kula volcanics, we see no compelling argument that their formation triggered this volcanism, given a lack of temporal correlation.

In eastern Turkey, the breakoff of the Bitlis slab that allowed the rise of primitive melts to the Anatolian upper plate is estimated to have occurred around 13–11 Ma (Keskin, 2003; Şengör et al., 2003). Geological data show that the East Anatolian fault was at least 6–5 Ma (Di Giuseppe et al., 2017; Karaoğlu et al., 2017). While some crustal thinning may have occurred due to transtensional tectonics, the region of most transtension, in the Cilicia basin to the west of Ceyhan-Osmaniye (Aksu et al., 2014), is devoid of magmatism, showing again no clear temporal and spatial link of tectonic processes and volcanism. Local tectonic triggers for deep melting in Karacadağ are even less clear. Although normal faults in the Arabian foreland may have facilitated the rise of the deep melts (Şengör & Yilmaz, 1981), the low amount of displacement makes it very unlikely that extension here caused deep melting.

The intraplate magmas of Turkey studied in this paper share a geochemical signature that resembles a mantle plume component. The asthenospheric signature we have defined is not the same throughout each of the volcanic centers, but chemical heterogeneity could have been readily introduced by local modification with overlying lithosphere, or simply the sheer size of, and thus heterogeneity in, the asthenospheric mantle component. In absence of hydration or decompression as a trigger for melting, we may thus explore whether heating is a viable mechanism, particularly for the Karacadağ and Ceyhan-Osmaniye volcanics, which appear to have formed in areas devoid of significant extension and formed at the modern plate boundary, or even south of it, within Arabia. That search invites inspection of scenarios involving mantle plumes as explanation for the melting of the Turkish intraplate volcanics. Mantle plumes are best known for massive outbursts of flood basalts (e.g., Ernst, 2014) followed by hotspot tracks that reflect plate motion relative to the

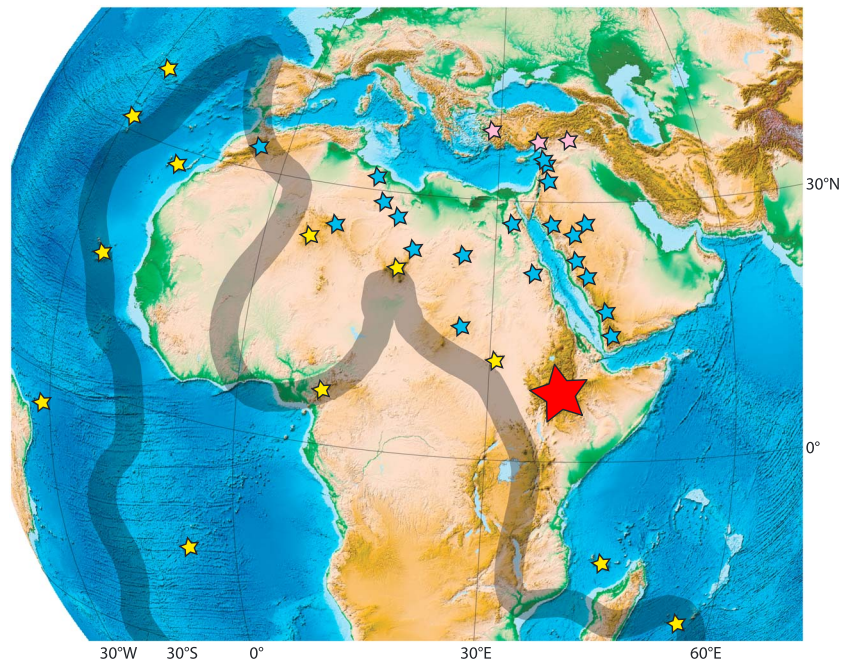


**Figure 11.** Outline of the large low shear wave velocity province (LLSVP) as indication for the plume generation zone sensu Burke et al. (2008). Red star = Afar large igneous province and active hotspot. Yellow stars = active hotspots as identified by Steinberger (2000). Blue stars = Neogene intraplate volcanic centers identified in the text. Pink stars = Anatolian intraplate volcanic centers studied in this paper.

underlying plume head (Morgan, 1971; Wilson, 1963). Additionally, plume head spreading (van Hinsbergen et al., 2011), or entrainment of plume material due to mantle flow (Faccenna et al., 2013), may produce diachronous trends in volcanism. The absence of a nearby flood basalts, or seismological evidence for a plume, or direct involvement of a deep-seated melt in the intraplate volcanics of Anatolia make that previously, correlation to a major plume was considered unlikely (e.g., Aldanmaz et al., 2000, 2006; Arger et al., 2000; Ekici et al., 2012, 2014; McKenzie & O’Nions, 1995; Pearce et al., 1990; Polat et al., 1997)—one of the key reasons why local deformation and slab edge formation have previously been invoked as triggers for melting in the first place. Faccenna et al. (2013) postulated that a northward younging trend of intraplate volcanism may exist from the Afar plume toward Anatolia, driven by mantle flow toward the Aegean rollback system, but at least on the scale of Anatolia, no clear diachronicity is visible.

Correlations between plate reconstructions placed in a mantle reference frames, and plume-related magmatism, however, have revealed that also small-scale volcanic centers may have a direct relationship with plumes, without clear diachronous trends. Modern hotspots and large igneous provinces linked to deep mantle plumes were shown to correlate within a belt of  $\sim 10^\circ$  around the edge of two large low shear wave velocity provinces (LLSVPs), below Africa and the Pacific—the “plume generation zone” (Burke et al., 2008; Burke & Torsvik, 2004)—and perhaps more when deflected in the direction of absolute plate motion, in the case of Africa-Arabia to the north (Faccenna et al., 2013). Later, however, not only such major volcanic provinces, but also kimberlites, that is, much smaller volume intraplate magmatic centers that form intraplate in regions of thick continental lithosphere, were shown to correlate with LLSVP edges in a region (Torsvik et al., 2010). Such smaller-scale centers may result from upward mantle convection dominated by upwelling along the edges of these LLSVPs and downwelling along major subduction systems between them (e.g., Becker & Faccenna, 2011).

Kimberlites only form where the mantle lithosphere is very thick. In places of thinner lithosphere, such lower-volume deeper-mantle upwellings (“mini-plumes”; e.g., Bosworth et al., 2015) would then produce a pattern of dispersed low-volume intraplate magmatic rocks, correlated with a zone around the edge of an LLSVP. So is there such a zone of intraplate volcanics in northern Africa and Arabia, in which Anatolia may

have become incorporated due to the opening of slab gaps that allowed the rise of miniplumes previously prevented by the downgoing slab?

Late Neogene low-volume, intraplate mafic volcanism, such as that found in Anatolia, is indeed found across a much wider area. Such volcanics are found across the Arabian peninsula, in Syria (Ma et al., 2013), Israel (Weinstein et al., 2006), Lebanon, Saudi Arabia (Abdel-Rahman & Nassar, 2004), and Jordan (Shaw et al., 2003), and also across North Africa, in Egypt (e.g., Abu El-Rus & Rooney, 2017; Endress et al., 2011), Sudan (Lucassen et al., 2013), Lybia (Bardintzeff et al., 2012; Radivojević et al., 2015), Chad (Deniel et al., 2015), Algeria (Azzouni-Sekkal et al., 2007; Beccaluva et al., 2007; Yahiaoui et al., 2014), and in the Atlas of Morocco (Anahnah et al., 2011), some of which were already marked as active hotspots by Steinberger (2000). In most cases, the locations of these volcanics display a correlation with local deformation structures, active or long inactive, but intraplate tectonics are very minor and do not provide a straightforward cause of melting, similar to our inference for Anatolia. The zone follows a  $\sim 20^\circ$  wide band around the northeastern edge of the African LLSVP, on the same order of magnitude as shown for kimberlites (Torsvik et al., 2010; Figure 11). Figure 11 shows the modern positions of the late Cenozoic intraplate volcanics, which due to northward absolute African plate motion have been displaced a few tens to hundreds of kilometers northward since formation. In addition, the pattern of intraplate volcanism may have been displaced northward due to northward mantle flow (e.g., Faccenna et al., 2013). We therefore tentatively postulate that “kimberlite-type” miniplumes may have triggered the melting of the intraplate magmatism, and the wider North African-Arabian volcanic province. The lithospheric thickness in North Africa and Arabia, and in our study area in Anatolia, is insufficiently thick to form kimberlites in Neogene times, but we suggest that these low-volume intraplate basalts were formed by a similar mechanism. This mechanism explains the nature and location of the Ceyhan-Osmaniye and Karacadağ volcanics. While a link between the Kula volcanics and mantle flow around a slab edge is not precluded, the presence of a slab gap below Kula would straightforwardly facilitate upward, miniplume-induced mantle flow to the base of the lithosphere, and we postulate that the volcanics in all of the studied areas in this paper are linked to the same, miniplume-related cause of melting, rather than local Anatolian geodynamics.

## 6. Conclusions

1. MI from Kula, Ceyhan-Osmaniye, and Karacadağ indicate the presence of diverse primitive melt compositions, which, independent of host olivine forsterite content, cannot be reconciled with simple fractionation processes. The observed variability in MI compositions is present in the most forsteritic olivines, essentially eliminating the effects of secondary processes that may have contributed to the diversity of melt compositions in later stages of magma evolution. Much of the compositional diversity can thus be taken as reflective of the heterogeneity of (near-)primary melts.
2. We observe the correlation between the compositional diversity of trapped melts and host groups based on olivine and spinel. In Kula rocks, olivine-spinel pairs corroborate the existence of two distinct compositional populations: Group 1 with high-CaO olivine and high-Cr# spinel (0.26–0.36) and Group 2 with low-CaO olivine and low-Cr# spinel (0.26–0.36). Ceyhan-Osmaniye rocks also host two distinct olivine-spinel groups, characterized by high-CaO olivines with high-Cr# spinel ( $\sim 0.16$ ) in Üçtepelers samples and low-CaO olivines with lower-Cr# spinel ( $\sim 0.06$ ) in Toprakkale samples. Karacadağ spinel inclusions are marked by significantly higher-Cr# spinel (0.39–0.52), coupled with lower olivine Fo content, than the other Anatolian volcanic centers.
3. Compositional diversity of Kula MI reflects mixing of two different parental melt components derived from the mantle source. End-member component A, which is most prevalent in Group 1, is characterized by low CaO content; high alkalinity and  $K_2O/TiO_2$ ,  $SiO_2$ ,  $Al_2O_3$ ,  $P_2O_5$ , and Cl content; and a more enriched trace element signature (e.g., La/Yb, Th/Yb, Nb/Yb, and Rb/Sr). Conversely, end-member component B, which is predominant in Group 2, is marked by opposite compositional characteristics.
4. Within Ceyhan-Osmaniye, we observe notable difference between Üçtepelers and Toprakkale parental melts. Üçtepelers MI display a relatively narrow compositional range, with high  $SiO_2$  and low  $K_2O/TiO_2$ ,  $K_2O$ ,  $P_2O_5$ ,  $TiO_2$ , and Cl content. In contrast, Toprakkale MI exhibit a considerably wider compositional range and contain a distinct population characterized by opposite compositional characteristics (OIB component). Trace elements in Toprakkale MI are considerably more enriched and display OIB-like incompatible trace element patterns, whereas Üçtepelers MI have lower abundances for most

incompatible elements and plot remarkably close to the mixing line between typical N-MORB and OIB compositions, showing affinity with highly enriched MORB (P-MORB-like) compositions (Gorring et al., 2003; McKenzie & Bickle, 1988; Pearce, 2014; Saccani et al., 2013, 2014).

5. The compositional diversity of Karacadağ parental melts also reflect mixing of two compositionally different end-member components. Parental melt component A is characterized by relatively low CaO content; high alkalinity and  $K_2O/TiO_2$ ,  $P_2O_5$ , and Cl content; and a more enriched trace element signature (e.g., Sr/Y, Sr, La, and Zr). Conversely, component B is marked by opposite characteristics: relatively high CaO content; lower alkalinity and  $K_2O/TiO_2$ ,  $P_2O_5$ , and Cl content; and less pronounced trace element enrichments.
6. Crystallization temperatures of 1280–1110 °C for olivines in Ceyhan-Osmaniye samples (Fo<sub>87–77</sub>) and 1255–1130 °C for olivines in Karacadağ samples (Fo<sub>85–75</sub>) are broadly similar. In contrast, Kula olivines show a large range of temperatures (1275–1090 °C) at narrow Fo (87–83 mol %) and MgO ranges, testifying to the mixing of compositionally diverse melts. Furthermore, oxygen fugacity values of the MI indicate oxidation states near the FMQ-NNO redox buffers for all studied samples.
7. MI from all studied volcanic centers show elemental ratios that testify to within-plate enrichment, rather than subduction zone enrichment or crustal contamination. Primitive Kula melts display a clear EM signature. In Ceyhan-Osmaniye, Toprakkale melts represent typical HIMU-OIB-type compositions, whereas Üçtepelers melts show a highly enriched MORB (P-MORB-like) compositions. Similar to Toprakkale, the mantle source beneath Karacadağ resembles typical HIMU-OIB compositions.
8. Calculations of the pressure and temperature conditions of primary melt generation yield 23–9 kbar and 1415–1215 °C for Kula, 28–19 kbar and 1430–1350 °C for Toprakkale (28–25 kbar and 1430–1390 °C for the OIB component), 23–18 kbar and 1400–1355 °C for Üçtepelers (P-MORB-like component), and 35–27 kbar and 1530–1455 °C for Karacadağ. The obtained pressures correspond to melt generation depths of 75–30 km for Kula, 90–65 km for Toprakkale (90–80 km for the OIB component), 75–60 km for Üçtepelers (P-MORB-like component), and 115–90 km for Karacadağ. In Ceyhan-Osmaniye, this supports a petrogenetic model in which ascending asthenosphere and shallower, depleted (MORB-type) mantle have interacted in variable degrees to give rise to a compositional continuum, ranging from OIB to P-MORB-like compositions.
9. The greatest depth of melting found in the MI of the Kula, Ceyhan-Osmaniye, and Karacadağ volcanics corresponds to the independently determined depth of the LAB in all three regions. The three regions are associated with either (1) no evidence for subduction (Karacadağ) or (2) a broken-off slab (Kula and Ceyhan-Osmaniye) that facilitated the rise of primitive asthenosphere to the base of the lithosphere. The rise of magma to the surface in all three regions was likely enabled by local deformation structures.
10. While gaps in the slabs and local deformation structures facilitated the formation of Anatolian intraplate volcanoes, these features all long predate the volcanism, and we see no clear cause-consequence relationship between slab deformation, crustal deformation, and intraplate volcanism.
11. We note that similar Late Neogene, low-volume, basaltic intraplate volcanism affected a much wider region including Arabia and North Africa, which is located within a belt of ~10° around the edge of the African LLSVP. We tentatively suggest that this volcanism was related to continuous deep-mantle upwelling along the LLSVP edges associated with whole-mantle convection and that the small-volume intraplate volcanics are linked to a miniplume-related cause of melting, similar to that responsible for kimberlites in cratonic regions. Regardless of their cause, we infer that the Anatolian intraplate volcanics are not a reflection of local Anatolian geodynamics but form part of a much wider Arabian-North African intraplate volcanic province, which was able to invade the Anatolian upper plate through slab gaps.

#### Acknowledgments

We gratefully acknowledge the help of Sergei Matveev and Tilly Bouten with EPMA analyses and Helen de Waard with LA-ICP-MS analyses. We thank Ercan Aldanmaz and one anonymous reviewer whose comments helped improve the paper. We also thank Laurent Jolivet for editorial handling. This research was supported by the Netherlands Research Centre for Integrated Solid Earth Science (ISES) through grant 6.2.12 and by the Olaf Schuiling Fund (Utrecht University Fund). I. K. N. and A. J. J. B. G. received funding from the European Research Council (ERC) under the European Union's Horizon 2020 research and innovation programme under grant agreement no. 759563 (ERC-StG ReVolutions). The data used are listed in the supporting information and references.

#### References

- Abdel-Rahman, A.-F. M., & Nassar, P. E. (2004). Cenozoic volcanism in the Middle East: Petrogenesis of alkali basalts from northern Lebanon. *Geological Magazine*, 141(5), 545–563. <https://doi.org/10.1017/S0016756804009604>
- Abu El-Rus, M. M. A., & Rooney, T. O. (2017). Insights into the lithosphere to asthenosphere melting transition in northeast Africa: Evidence from the Tertiary volcanism in middle Egypt. *Chemical Geology*, 455, 282–303. <https://doi.org/10.1016/J.CHEMGEO.2016.10.005>
- Agostini, S., Doglioni, C., Innocenti, F., Manetti, P., Tonarini, S., & Savaşçın, M. Y. (2007). The transition from subduction-related to intraplate Neogene magmatism in the western Anatolia and Aegean area. *Geological Society of America, Special Paper*, 418, 1–15. [https://doi.org/10.1130/2007.2418\(01\)](https://doi.org/10.1130/2007.2418(01))

- Aksu, A. E., Walsh-Kennedy, S., Hall, J., Hiscott, R. N., Yaltrak, C., Akhun, S. D., & Çifçi, G. (2014). The Pliocene–Quaternary tectonic evolution of the Cilicia and Adana basins, eastern Mediterranean: Special reference to the development of the Kozan Fault zone. *Tectonophysics*, 622, 22–43. <https://doi.org/10.1016/J.TECTO.2014.03.025>
- Aldanmaz, E. (2002). Mantle source characteristics of alkali basalts and basanites in an extensional intracontinental plate setting, western Anatolia, Turkey: Implications for multi-stage melting. *International Geology Review*, 44(5), 440–457. <https://doi.org/10.2747/0020-6814.44.5.440>
- Aldanmaz, E., Gourgaud, A., & Kaymakci, N. (2005). Constraints on the composition and thermal structure of the upper mantle beneath NW Turkey: Evidence from mantle xenoliths and alkali primary melts. *Journal of Geodynamics*, 39(3), 277–316.
- Aldanmaz, E., Köprübaşı, N., Gürer, Ö. F., Kaymakçı, N., & Gourgaud, A. (2006). Geochemical constraints on the Cenozoic, OIB-type alkaline volcanic rocks of NW Turkey: Implications for mantle sources and melting processes. *Lithos*, 86(1–2), 50–76. <https://doi.org/10.1016/j.lithos.2005.04.003>
- Aldanmaz, E., Pearce, J. A., Thirlwall, M. F., & Mitchell, J. G. (2000). Petrogenetic evolution of late Cenozoic, post-collision volcanism in western Anatolia, Turkey. *Journal of Volcanology and Geothermal Research*, 102(1–2), 67–95. [https://doi.org/10.1016/S0377-0273\(00\)00182-7](https://doi.org/10.1016/S0377-0273(00)00182-7)
- Aldanmaz, E., Pickard, M., Meisel, T., Altunkaynak, Ş., Sayit, K., Şen, P., et al. (2015). Source components and magmatic processes in the genesis of Miocene to Quaternary lavas in western Turkey: Constraints from HSE distribution and Hf–Pb–Os isotopes. *Contributions to Mineralogy and Petrology*, 170(2). <https://doi.org/10.1007/s00410-015-1176-x>
- Alici, P., Temel, A., & Gourgaud, A. (2002). Pb–Nd–Sr isotope and trace element geochemistry of Quaternary extension-related alkaline volcanism: A case study of Kula region (western Anatolia, Turkey). *Journal of Volcanology and Geothermal Research*, 115(3–4), 487–510. [https://doi.org/10.1016/S0377-0273\(01\)00328-6](https://doi.org/10.1016/S0377-0273(01)00328-6)
- Alici, P., Temel, A., Gourgaud, A., Vidal, P., & Gündoğdu, M. N. (2001). Quaternary tholeiitic to alkaline volcanism in the Karasu Valley, Dead Sea Rift Zone, Southeast Turkey: Sr–Nd–Pb–O isotopic and trace-element approaches to crust–mantle interaction. *International Geology Review*, 43(2), 120–138. <https://doi.org/10.1080/00206810109465004>
- Allen, M. B., Jackson, J. C., & Walker, R. W. (2004). Late Cenozoic reorganization of the Arabia–Eurasia collision and the comparison of short-term and long-term deformation rates. *Tectonics*, 23, TC2008. <https://doi.org/10.1029/2003TC001530>
- Anahnah, F., Galindo-Zaldívar, J., Chalouan, A., Pedrera, A., Ruano, P., Pous, J., et al. (2011). Deep resistivity cross section of the intraplate Atlas Mountains (NW Africa): New evidence of anomalous mantle and related Quaternary volcanism. *Tectonics*, 30, TC5014. <https://doi.org/10.1029/2010TC002859>
- Angus, D. A., Wilson, D. C., Sandvol, E., & Ni, J. F. (2006). Lithospheric structure of the Arabian and Eurasian collision zone in eastern Turkey from S-wave receiver functions. *Geophysical Journal International*, 166(3), 1335–1346. <https://doi.org/10.1111/j.1365-246X.2006.03070.x>
- Arai, S. (1994). Characterization of spinel peridotites by olivine–spinel compositional relationships: Review and interpretation. *Chemical Geology*, 113(3–4), 191–204. [https://doi.org/10.1016/0009-2541\(94\)90066-3](https://doi.org/10.1016/0009-2541(94)90066-3)
- Arger, J., Mitchell, J., & Westaway, R. W. C. (2000). Neogene and Quaternary volcanism of southeastern Turkey. *Geological Society, London, Special Publications*, 173(1), 459–487. <https://doi.org/10.1144/GSL.SP.2000.173.01.22>
- Azzouni-Sekkal, A., Bonin, B., Benhallou, B., Yahiaoui, R., & Liégeois, J.-P. (2007). Cenozoic alkaline volcanism of the Atakor massif, Hoggar, Algeria. *Geological Society of America, Special Paper*, 418, 321–340. [https://doi.org/10.1130/2007.2418\(16\)](https://doi.org/10.1130/2007.2418(16))
- Bağcı, U., Alpaslan, M., Frei, R., Kurt, M. A., & Temel, A. (2011). Different degrees of partial melting of the enriched mantle source for Plio–Quaternary basic volcanism, Toprakale (Osmaniye) Region, Southern Turkey. *Turkish Journal of Earth Sciences*, 20(1), 115–135. <https://doi.org/10.3906/Yer-1003-30>
- Bardintzeff, J.-M., Deniel, C., Guillou, H., Platevoet, B., Télouk, P., & Oun, K. M. (2012). Miocene to recent alkaline volcanism between Al Haruj and Waw an Namous (southern Libya). *International Journal of Earth Sciences*, 101(4), 1047–1063. <https://doi.org/10.1007/s00531-011-0708-5>
- Beccaluva, L., Azzouni-Sekkal, A., Benhallou, B., Bianchini, G., Ellam, R. M., Marzola, M., et al. (2007). Intracratonic asthenosphere upwelling and lithosphere rejuvenation beneath the Hoggar swell (Algeria): Evidence from HIMU metasomatised Iherzolite mantle xenoliths. *Earth and Planetary Science Letters*, 260(3–4), 482–494. <https://doi.org/10.1016/J.EPSL.2007.05.047>
- Beccaluva, L., Bianchini, G., Natali, C., & Siena, F. (2009). Continental flood basalts and mantle plumes: A case study of the northern Ethiopian Plateau. *Journal of Petrology*, 50(7), 1377–1403. <https://doi.org/10.1093/ptrology/egp024>
- Becker, T. W., & Faccenna, C. (2011). Mantle conveyor beneath the Tethyan collisional belt. *Earth and Planetary Science Letters*, 310(3–4), 453–461. <https://doi.org/10.1016/J.EPSL.2011.08.021>
- Berk Biryol, C., Beck, S. L., Zandt, G., & Özacar, A. A. (2011). Segmented African lithosphere beneath the Anatolian region inferred from teleseismic P-wave tomography. *Geophysical Journal International*, 184(3), 1037–1057. <https://doi.org/10.1111/j.1365-246X.2010.04910.x>
- Bilgin, A. Z., & Ercan, T. (1981). Petrology of the Quaternary basalts of Iskenderun Gulf Osmaniye area. *Bulletin of the Geological Society of Turkey*, 24, 21–30.
- Bocchini, G. M., Brüstle, A., Becker, D., Meier, T., van Keken, P. E., Ruscic, M., et al. (2018). Tearing, segmentation, and backstepping of subduction in the Aegean: New insights from seismicity. *Tectonophysics*, 734–735, 96–118. <https://doi.org/10.1016/J.TECTO.2018.04.002>
- Borisov, A. A., & Shapkin, A. I. (1989). A new empirical equation rating Fe<sup>3+</sup>/Fe<sup>2+</sup> in magmas to their composition, oxygen fugacity, and temperature. *Geokhimiya*, 6, 892–897.
- Bosworth, W., Stockli, D. F., & Helgeson, D. E. (2015). Integrated outcrop, 3D seismic, and geochronologic interpretation of Red Sea dike-related deformation in the Western Desert, Egypt – The role of the 23 Ma Cairo “mini-plume”. *Journal of African Earth Sciences*, 109, 107–119. <https://doi.org/10.1016/J.JAFREARSCI.2015.05.005>
- Bozkurt, E., & Oberhänsli, R. (2001). Menderes Massif (western Turkey): Structural, metamorphic and magmatic evolution - a synthesis. *International Journal of Earth Sciences*, 89(4), 679–708. <https://doi.org/10.1007/s005310000173>
- Brun, J.-P., & Sokoutis, D. (2010). 45 m.y. of Aegean crust and mantle flow driven by trench retreat. *Geology*, 38(9), 815–818. <https://doi.org/10.1130/G30950.1>
- Bunbury, J. M., Hall, L., Anderson, G. J., & Stannard, A. (2001). The determination of fault movement history from the interaction of local drainage with volcanic episodes. *Geological Magazine*, 138(2), 185–192. <https://doi.org/10.1017/S0016756801005271>
- Burke, K., Steinberger, B., Torsvik, T. H., & Smethurst, M. A. (2008). Plume generation zones at the margins of large low shear velocity provinces on the core–mantle boundary. *Earth and Planetary Science Letters*, 265(1–2), 49–60. <https://doi.org/10.1016/J.EPSL.2007.09.042>
- Burke, K., & Torsvik, T. H. (2004). Derivation of large igneous provinces of the past 200 million years from long-term heterogeneities in the deep mantle. *Earth and Planetary Science Letters*, 227(3–4), 531–538. <https://doi.org/10.1016/J.EPSL.2004.09.015>
- Çapan, U. Z., Vidal, P., & Cantagrel, J. M. (1987). Kr–Ar, Nd, Sr and Pb isotopic study of Quaternary volcanism in Karasu (Hatay), N-end of Dead Sea rift zone in SE-Turkey. *Yerbilimleri Dergisi*, 14, 165.
- Cesur, D., Mutlu, H., Aldanmaz, E., Güleç, N., Stuart, F., & Sariöz, K. (2016). Major and trace element concentrations of Kula volcanics and investigation of source composition. *Geophysical Research Abstracts*, 18(112), 7490.

- Chakrabarti, R., Basu, A. R., & Ghatak, A. (2012). Chemical geodynamics of western Anatolia. *International Geology Review*, 54(2), 227–248. <https://doi.org/10.1080/00206814.2010.543787>
- Çoban, H. (2007). Basalt magma genesis and fractionation in collision- and extension-related provinces: A comparison between eastern, central and western Anatolia. *Earth-Science Reviews*, 80(3–4), 219–238. <https://doi.org/10.1016/j.earscirev.2006.08.006>
- Danyushevsky, L. V. (2001). The effect of small amounts of H<sub>2</sub>O on crystallisation of mid-ocean ridge and backarc basin magmas. *Journal of Volcanology and Geothermal Research*, 110(3–4), 265–280. [https://doi.org/10.1016/S0377-0273\(01\)00213-X](https://doi.org/10.1016/S0377-0273(01)00213-X)
- Danyushevsky, L. V., Della-Pasqua, F. N., & Sokolov, S. (2000). Re-equilibration of melt inclusions trapped by magnesian olivine phenocrysts from subduction-related magmas: Petrological implications. *Contributions to Mineralogy and Petrology*, 138(1), 68–83. <https://doi.org/10.1007/PL00007664>
- Danyushevsky, L. V., McNeill, A. W., & Sobolev, A. V. (2002). Experimental and petrological studies of melt inclusions in phenocrysts from mantle-derived magmas: An overview of techniques, advantages and complications. *Chemical Geology*, 183(1–4), 5–24. [https://doi.org/10.1016/S0009-2541\(01\)00369-2](https://doi.org/10.1016/S0009-2541(01)00369-2)
- Danyushevsky, L. V., & Plechov, P. (2011). Petrolog3: Integrated software for modeling crystallization processes. *Geochemistry, Geophysics, Geosystems*, 12, Q07021. <https://doi.org/10.1029/2011GC003516>
- Danyushevsky, L. V., & Sobolev, A. V. (1996). Ferric-ferrous ratio and oxygen fugacity calculations for primitive mantle-derived melts: Calibration of an empirical technique. *Mineralogy and Petrology*, 57(3–4), 229–241. <https://doi.org/10.1007/BF01162360>
- Danyushevsky, L. V., Sokolov, S., & Falloon, T. J. (2002). Melt inclusions in olivine phenocrysts: Using diffusive re-equilibration to determine the cooling history of a crystal, with implications for the origin of olivine-phyric volcanic rocks. *Journal of Petrology*, 43(9), 1651–1671. <https://doi.org/10.1093/ptrology/43.9.1651>
- de Hoog, J. C. M., Mason, P. R. D., & van Bergen, M. J. (2001). Sulfur and chalcophile elements in subduction zones: Constraints from a laser ablation ICP-MS study of melt inclusions from Galunggung volcano, Indonesia. *Geochimica et Cosmochimica Acta*, 65(18), 3147–3164. [https://doi.org/10.1016/S0016-7037\(01\)00634-2](https://doi.org/10.1016/S0016-7037(01)00634-2)
- Deniel, C., Vincent, P. M., Beauvilain, A., & Gourgaud, A. (2015). The Cenozoic volcanic province of Tibesti (Sahara of Chad): Major units, chronology, and structural features. *Bulletin of Volcanology*, 77(9), 74. <https://doi.org/10.1007/s00445-015-0955-6>
- Dewey, J. F., Hempton, M. R., Kidd, W. S. F., Şaroğlu, F., & Şengör, A. M. C. (1986). Shortening of continental lithosphere: The neotectonics of Eastern Anatolia—A young collision zone. *Geological Society, London, Special Publications*, 19(1), 1–36.
- Di Giuseppe, P., Agostini, S., Lustrino, M., Karaoğlu, Ö., Savaşçın, M. Y., Manetti, P., & Ersoy, Y. (2017). Transition from compression to strike-slip tectonics revealed by Miocene–Pleistocene volcanism west of the Karlova triple junction (East Anatolia). *Journal of Petrology*, 58(10), 2055–2087. <https://doi.org/10.1093/ptrology/egx082>
- Dilek, Y., & Altunkaynak, Ş. (2007). Cenozoic crustal evolution and mantle dynamics of post-collisional magmatism in western Anatolia. *International Geology Review*, 49(5), 431–453. <https://doi.org/10.2747/0020-6814.49.5.431>
- Dilek, Y., & Altunkaynak, Ş. (2009). Geochemical and temporal evolution of Cenozoic magmatism in western Turkey: Mantle response to collision, slab break-off, and lithospheric tearing in an orogenic belt. *Geological Society, London, Special Publications*, 311(1), 213–233. <https://doi.org/10.1144/SP311.8>
- Dilek, Y., & Altunkaynak, Ş. (2010). Geochemistry of Neogene–Quaternary alkaline volcanism in western Anatolia, Turkey, and implications for the Aegean mantle. *International Geology Review*, 52(4–6), 631–655. <https://doi.org/10.1080/00206810903495020>
- Dilek, Y., Altunkaynak, Ş., & Öner, Z. (2009). Syn-extensional granitoids in the Menderes core complex and the late Cenozoic extensional tectonics of the Aegean province. *Geological Society, London, Special Publications*, 321(1), 197–223.
- Dyer, J. M. (1987). Petrology of the Kula Volcanic Field, western Turkey, (Master's thesis). State Univ. of New York at Albany.
- Ekici, T., Macpherson, C. G., & Otlu, N. (2012). Polybaric melting of a single mantle source during the Neogene Siverek phase of the Karacadağ Volcanic Complex, SE Turkey. *Lithos*, 146–147, 152–163. <https://doi.org/10.1016/j.lithos.2012.05.004>
- Ekici, T., Macpherson, C. G., Otlu, N., & Fontignie, D. (2014). Foreland magmatism during the Arabia–Eurasia collision: Pliocene–Quaternary activity of the Karacadağ Volcanic Complex, SW Turkey. *Journal of Petrology*, 55(9), 1753–1777. <https://doi.org/10.1093/ptrology/egu040>
- Elitok, Ö., & Dolmaz, M. N. (2008). Mantle flow-induced crustal thinning in the area between the easternmost part of the Anatolian plate and the Arabian foreland (E Turkey) deduced from the geological and geophysical data. *Gondwana Research*, 13(3), 302–318. <https://doi.org/10.1016/j.gr.2007.08.007>
- Endress, C., Furman, T., El-Rus, M. A. A., & Hanan, B. B. (2011). Geochemistry of 24 Ma basalts from NE Egypt: Source components and fractionation history. *Geological Society, London, Special Publications*, 357(1), 265–283. <https://doi.org/10.1144/SP357.14>
- Ercan, T. (1982). Kula yöresinin jeolojisi ve volkanitlerin petrolojisi. *Istanbul Yerbilimleri Dergisi*, 3(1–2), 77–124.
- Ercan, T. (1993). Interpretation of geochemical, radiometric and isotopic data on Kula volcanics (Manisa-W. Anatolia). *Geological Bulletin of Turkey*, 36, 113–129.
- Ercan, T., Fujitani, T., Madsuda, J.-I., Notsu, K., & Ui, T. (1990). Doğu ve Güneydoğu Anadolu Neojen-Kuvaterner volkanitlerine ilişkin yeni jeokimyasal, radyometrik ve izotopik verilerin yorumu. *Maden Tetkik ve Arama Dergisi*, 110, 143–164.
- Ercan, T., Şaroğlu, F., Turhan, N., Matsuda, J. I., Fujitani, T., Notsu, K., et al. (1991). The geology and petrology of the Karacadağ volcanites. *Bulletin of the Geological Congress of Turkey*, 6, 118–133.
- Ercan, T., Satir, M., Steinitz, G., Dora, A., Sarifakioglu, E., Adis, C., et al. (1995). Characteristics of the tertiary volcanism in the Biga Peninsula, Gökceada, Bozcaada and Tavşanadası, NW Anatolia. *Bulletin. Mineral Research and Exploration Institute (Turkey)*, 117, 55–86.
- Ernst, R. E. (2014). *Large igneous provinces*. Cambridge University Press. <https://doi.org/10.1017/CBO9781139025300>
- Ersoy, Y. E., Helvacı, C., & Palmer, M. R. (2012). Petrogenesis of the Neogene volcanic units in the NE–SW-trending basins in western Anatolia, Turkey. *Contributions to Mineralogy and Petrology*, 163(3), 379–401. <https://doi.org/10.1007/s00410-011-0679-3>
- Faccenna, C., Becker, T. W., Jolivet, L., & Keskin, M. (2013). Mantle convection in the Middle East: Reconciling Afar upwelling, Arabia indentation and Aegean trench rollback. *Earth and Planetary Science Letters*, 375, 254–269. <https://doi.org/10.1016/j.epsl.2013.05.043>
- Faccenna, C., Bellier, O., Martinod, J., Pìromallo, C., & Regard, V. (2006). Slab detachment beneath eastern Anatolia: A possible cause for the formation of the North Anatolian fault. *Earth and Planetary Science Letters*, 108(B2), 1–2. <https://doi.org/10.1029/2002JB001757>
- Falloon, T. J., Green, D. H., Hatton, C. J., & Harris, K. L. (1988). Anhydrous partial melting of a fertile and depleted peridotite from 2 to 30 kb and application to basalt petrogenesis. *Journal of Petrology*, 29(6), 1257–1282. <https://doi.org/10.1093/ptrology/29.6.1257>
- Ford, C. E., Russell, D. G., Craven, J. A., & Fisk, M. R. (1983). Olivine-liquid equilibria: Temperature, pressure and composition dependence of the crystal/liquid cation partition coefficients for Mg, Fe<sup>2+</sup>, Ca and Mn. *Journal of Petrology*, 24(3), 256–266. <https://doi.org/10.1093/ptrology/24.3.256>

- Gessner, K., Gallardo, L. A., Markwitz, V., Ring, U., & Thomson, S. N. (2013). What caused the denudation of the Menderes Massif: Review of crustal evolution, lithosphere structure, and dynamic topography in southwest Turkey. *Gondwana Research*, 24(1), 243–274. <https://doi.org/10.1016/J.GR.2013.01.005>
- Gorring, M., Singer, B., Gowers, J., & Kay, S. M. (2003). Plio–Pleistocene basalts from the Meseta del Lago Buenos Aires, Argentina: Evidence for asthenosphere–lithosphere interactions during slab window magmatism. *Chemical Geology*, 193(3–4), 215–235. [https://doi.org/10.1016/S0009-2541\(02\)00249-8](https://doi.org/10.1016/S0009-2541(02)00249-8)
- Grützner, T., Prelević, D., & Akal, C. (2013). Geochemistry and origin of ultramafic enclaves and their basanitic host rock from Kula Volcano, Turkey. *Lithos*, 180–181, 58–73. <https://doi.org/10.1016/j.lithos.2013.08.001>
- Güleç, N. (1991). Crust–mantle interaction in western Turkey: Implications from Sr and Nd isotope geochemistry of Tertiary and Quaternary volcanics. *Geological Magazine*, 128(05), 417–435. <https://doi.org/10.1017/S0016756800018604>
- Gürer, D., Plunder, A., Kirst, F., Corfu, F., Schmid, S. M., & van Hinsbergen, D. J. J. (2018). A long-lived Late Cretaceous–early Eocene extensional province in Anatolia? Structural evidence from the Ivriz Detachment, southern central Turkey. *Earth and Planetary Science Letters*, 481, 111–124. <https://doi.org/10.1016/J.EPSL.2017.10.008>
- Gürer, D., & van Hinsbergen, D. J. J. (2018). Diachronous demise of the Neotethys Ocean as a driver for non-cylindrical orogenesis in Anatolia. *Tectonophysics*. <https://doi.org/10.1016/J.TECTO.2018.06.005>
- Gürsoy, H., Tatar, O., Piper, J. D. A., Heimann, A., Koçbulut, F., & Mesci, B. L. (2009). Palaeomagnetic study of Tertiary volcanic domains in Southern Turkey and Neogene anticlockwise rotation of the Arabian Plate. *Tectonophysics*, 465(1–4), 114–127. <https://doi.org/10.1016/j.tecto.2008.11.001>
- Gürsoy, H., Tatar, O., Piper, J. D. A., Heimann, A., & Mesci, L. (2003). Neotectonic deformation linking the east Anatolian and Karataş-Osmaniye intracontinental transform fault zones in the Gulf of İskenderun, southern Turkey, deduced from paleomagnetic study of the Ceyhan-Osmaniye volcanics. *Tectonics*, 22(6), 1067. <https://doi.org/10.1029/2003TC001524>
- Hafkenschied, E., Wortel, M. J. R., & Spakman, W. (2006). Subduction history of the Tethyan region derived from seismic tomography and tectonic reconstructions. *Journal of Geophysical Research*, 111, B08401. <https://doi.org/10.1029/2005JB003791>
- Hirose, K., & Kushiro, I. (1993). Partial melting of dry peridotites at high pressures: Determination of compositions of melts segregated from peridotite using aggregates of diamond. *Earth and Planetary Science Letters*, 114(4), 477–489. [https://doi.org/10.1016/0012-821X\(93\)90077-M](https://doi.org/10.1016/0012-821X(93)90077-M)
- Holness, M. B., & Bunbury, J. M. (2006). Insights into continental rift-related magma chambers: Cognate nodules from the Kula Volcanic Province, western Turkey. *Journal of Volcanology and Geothermal Research*, 153(3–4), 241–261. <https://doi.org/10.1016/j.jvolgeores.2005.12.004>
- Hüsing, S. K., Zachariasse, W. J., van Hinsbergen, D. J. J., Krijgsman, W., Inceöz, M., Harzhauser, M., et al. (2009). Oligocene–Miocene basin evolution in SE Anatolia, Turkey: Constraints on the closure of the eastern Tethys gateway. *Geological Society, London, Special Publications*, 311(1), 107–132. <https://doi.org/10.1144/SP311.4>
- Ilani, S., Harlavan, Y., Tarawneh, K., Rabba, I., Weinberger, R., Ibrahim, K., et al. (2001). New K–Ar ages of basalts from the Harrat Ash Shaam volcanic field in Jordan: Implications for the span and duration of the upper-mantle upwelling beneath the western Arabian plate. *Geology*, 29(2), 171–174. [https://doi.org/10.1130/0091-7613\(2001\)029<0171:NKAAOB>2.0.CO;2](https://doi.org/10.1130/0091-7613(2001)029<0171:NKAAOB>2.0.CO;2)
- Innocenti, F., Agostini, S., Di Vincenzo, G., Doglioni, C., Manetti, P., Savaşçın, M. Y., & Tonarini, S. (2005). Neogene and Quaternary volcanism in western Anatolia: Magma sources and geodynamic evolution. *Marine Geology*, 221(1–4), 397–421. <https://doi.org/10.1016/j.margeo.2005.03.016>
- Italiano, F., Yuce, G., di Bella, M., Rojay, B., Sabatino, G., Tripodo, A., et al. (2017). Noble gases and rock geochemistry of alkaline intraplate volcanics from the Amik and Ceyhan-Osmaniye areas, SE Turkey. *Chemical Geology*, 469, 34–46. <https://doi.org/10.1016/j.chemgeo.2017.04.003>
- Jackson, M. G., & Hart, S. R. (2006). Strontium isotopes in melt inclusions from Samoan basalts: Implications for heterogeneity in the Samoan plume. *Earth and Planetary Science Letters*, 245(1–2), 260–277. <https://doi.org/10.1016/J.EPSL.2006.02.040>
- Jochum, K. P., Weis, U., Stoll, B., Kuzmin, D., Yang, Q., Raczek, I., et al. (2011). Determination of reference values for NIST SRM 610–617 glasses following ISO guidelines. *Geostandards and Geoanalytical Research*, 35(4), 397–429. <https://doi.org/10.1111/j.1751-908X.2011.00120.x>
- Jolivet, L., & Brun, J.-P. (2010). Cenozoic geodynamic evolution of the Aegean. *International Journal of Earth Sciences*, 99(1), 109–138. <https://doi.org/10.1007/s00531-008-0366-4>
- Jolivet, L., Menant, A., Sternai, P., Rabillard, A., Arbaret, L., Augier, R., et al. (2015). The geological signature of a slab tear below the Aegean. *Tectonophysics*, 659, 166–182. <https://doi.org/10.1016/J.TECTO.2015.08.004>
- Karaoğlu, Ö., & Helvacı, C. (2014). Isotopic evidence for a transition from subduction to slab-tear related volcanism in western Anatolia, Turkey. *Lithos*, 192–195, 226–239. <https://doi.org/10.1016/j.lithos.2014.02.006>
- Karaoğlu, Ö., Selçuk, A. S., & Gudmundsson, A. (2017). Tectonic controls on the Karlova triple junction (Turkey): Implications for tectonic inversion and the initiation of volcanism. *Tectonophysics*, 694, 368–384. <https://doi.org/10.1016/J.TECTO.2016.11.018>
- Keskin, M. (2003). Magma generation by slab steepening and breakoff beneath a subduction-accretion complex: An alternative model for collision-related volcanism in eastern Anatolia, Turkey. *Geophysical Research Letters*, 30(24), 8046. <https://doi.org/10.1029/2003GL018019>
- Keskin, M. (2007). Eastern Anatolia: A hot spot in a collision zone without a mantle plume. *Geological Society of America, Special Paper*, 430, 693–722.
- Keskin, M., Chugaev, A. V., Lebedev, V. A., Sharkov, E. V., Oyan, V., & Kavak, O. (2012a). The geochronology and origin of mantle sources for late Cenozoic intraplate volcanism in the frontal part of the Arabian plate in the Karacadağ neovolcanic area of Turkey. Part 1. The results of isotope-geochronological studies. *Journal of Volcanology and Seismology*, 6(6), 352–360. <https://doi.org/10.1134/S0742046312060036>
- Keskin, M., Chugaev, A. V., Lebedev, V. A., Sharkov, E. V., Oyan, V., & Kavak, O. (2012b). The geochronology and origin of mantle sources for late Cenozoic intraplate volcanism in the frontal part of the Arabian plate in the Karacadağ neovolcanic area of Turkey. Part 2. The results of geochemical and isotope (Sr–Nd–Pb) studies. *Journal of Volcanology and Seismology*, 6(6), 361–382. <https://doi.org/10.1134/S0742046312060048>
- Keskin, M., Pearce, J. A., & Mitchell, J. G. (1998). Volcano-stratigraphy and geochemistry of collision-related volcanism on the Erzurum-Kars Plateau, northeastern Turkey. *Journal of Volcanology and Geothermal Research*, 85(1–4), 355–404. [https://doi.org/10.1016/S0377-0273\(98\)00063-8](https://doi.org/10.1016/S0377-0273(98)00063-8)
- Kind, R., Eken, T., Tilmann, F., Sodoudi, F., Taymaz, T., Bulut, F., et al. (2015). Thickness of the lithosphere beneath Turkey and surroundings from S-receiver functions. *Solid Earth*, 6(3), 971–984. <https://doi.org/10.5194/se-6-971-2015>
- Klaver, M., Davies, G. R., & Vroon, P. Z. (2016). Subslab mantle of African provenance infiltrating the Aegean mantle wedge. *Geology*, 44(5), 367–370. <https://doi.org/10.1130/G37627.1>

- Koç, A., & Kaymakçı, N. (2013). Kinematics of Sürgü Fault Zone (Malatya, Turkey): A remote sensing study. *Journal of Geodynamics*, *65*, 292–307. <https://doi.org/10.1016/J.JOG.2012.08.001>
- Koçbulut, F., Akpınar, Z., Tatar, O., Piper, J. D. A., & Roberts, A. P. (2013). Palaeomagnetic study of the Karacadağ Volcanic Complex, SE Turkey: Monitoring Neogene anticlockwise rotation of the Arabian Plate. *Tectonophysics*, *608*, 1007–1024. <https://doi.org/10.1016/j.tecto.2013.07.013>
- Koornneef, J. M., Nikogosian, I. K., van Bergen, M. J., Smeets, R., Bouman, C., & Davies, G. R. (2015). TIMS analysis of Sr and Nd isotopes in melt inclusions from Italian potassium-rich lavas using prototype  $10^{13} \Omega$  amplifiers. *Chemical Geology*, *397*, 14–23. <https://doi.org/10.1016/j.chemgeo.2015.01.005>
- Krienitz, M.-S., Haase, K. M., Mezger, K., Eckardt, V., & Shaikh-Mashail, M. A. (2006). Magma genesis and crustal contamination of continental intraplate lavas in northwestern Syria. *Contributions to Mineralogy and Petrology*, *151*(6), 698–716.
- Krienitz, M.-S., Haase, K. M., Mezger, K., & Shaikh-Mashail, M. A. (2007). Magma genesis and mantle dynamics at the Harrat Ash Shamah volcanic field (southern Syria). *Journal of Petrology*, *48*(8), 1513–1542.
- Krienitz, M.-S., Haase, K. M., Mezger, K., van den Bogaard, P., Thiemann, V., & Shaikh-Mashail, M. A. (2009). Tectonic events, continental intraplate volcanism, and mantle plume activity in northern Arabia: Constraints from geochemistry and Ar-Ar dating of Syrian lavas. *Geochemistry, Geophysics, Geosystems*, *10*, Q04008. <https://doi.org/10.1029/2008GC002254>
- Le Bas, M. J., Le Maitre, R. W., Streckeisen, A., & Zanettin, B. (1986). A chemical classification of volcanic rocks based on the total alkali-silica diagram. *Journal of Petrology*, *27*(3), 745–750. <https://doi.org/10.1093/ptrology/27.3.745>
- Lucassen, F., Pudlo, D., Franz, G., Romer, R. L., & Dulski, P. (2013). Cenozoic intra-plate magmatism in the Darfur volcanic province: Mantle source, phonolite-trachyte genesis and relation to other volcanic provinces in NE Africa. *International Journal of Earth Sciences*, *102*(1), 183–205. <https://doi.org/10.1007/s00531-012-0792-1>
- Lustrino, M., Keskin, M., Mattioli, M., & Kavak, O. (2012). Heterogeneous mantle sources feeding the volcanic activity of Mt. Karacadağ (SE Turkey). *Journal of Asian Earth Sciences*, *46*, 120–139. <https://doi.org/10.1016/j.jseas.2011.11.016>
- Lustrino, M., Keskin, M., Mattioli, M., Lebedev, V. A., Chugayev, A., Sharkov, E., & Kavak, O. (2010). Early activity of the largest Cenozoic shield volcano in the circum-Mediterranean area: Mt. Karacadağ, SE Turkey. *European Journal of Mineralogy*, *22*(3), 343–362. <https://doi.org/10.1127/0935-1221/2010/0022-2024>
- Lustrino, M., & Sharkov, E. (2006). Neogene volcanic activity of western Syria and its relationship with Arabian plate kinematics. *Journal of Geodynamics*, *42*, 115–139. <https://doi.org/10.1016/j.jog.2006.06.003>
- Lustrino, M., & Wilson, M. (2007). The circum-Mediterranean anorogenic Cenozoic igneous province. *Earth-Science Reviews*, *81*(1–2), 1–65. <https://doi.org/10.1016/j.earscirev.2006.09.002>
- Ma, G. S.-K., Malpas, J., Suzuki, K., Lo, C.-H., Wang, K.-L., Iizuka, Y., & Xenophontos, C. (2013). Evolution and origin of the Miocene intraplate basalts on the Aleppo Plateau, NW Syria. *Chemical Geology*, *335*, 149–171. <https://doi.org/10.1016/J.CHEMGEO.2012.11.001>
- Ma, G. S.-K., Malpas, J., Xenophontos, C., & Chan, G. H.-N. (2011). Petrogenesis of latest miocene-quaternary continental intraplate volcanism along the northern Dead Sea Fault System (Al Ghab-Homs volcanic field), western Syria: Evidence for lithosphere-asthenosphere interaction. *Journal of Petrology*, *52*(2), 401–430. <https://doi.org/10.1093/ptrology/egq085>
- MacLennan, J. (2008). Lead isotope variability in olivine-hosted melt inclusions from Iceland. *Geochimica et Cosmochimica Acta*, *72*(16), 4159–4176. <https://doi.org/10.1016/j.gca.2008.05.034>
- Maddy, D., Schreve, D., Demir, T., Veldkamp, A., Wijbrans, J. R., van Gorp, W., et al. (2015). The earliest securely-dated hominin artefact in Anatolia? *Quaternary Science Reviews*, *109*, 68–75. <https://doi.org/10.1016/J.QUASCIREV.2014.11.021>
- Maddy, D., Veldkamp, A., Demir, T., van Gorp, W., Wijbrans, J. R., van Hinsbergen, D. J. J., et al. (2017). The Gediz River fluvial archive: A benchmark for Quaternary research in western Anatolia. *Quaternary Science Reviews*, *166*, 289–306. <https://doi.org/10.1016/J.QUASCIREV.2016.07.031>
- Mahmoud, Y., Masson, F., Meghraoui, M., Cakir, Z., Alchalbi, A., Yavasoglu, H., et al. (2013). Kinematic study at the junction of the East Anatolian fault and the Dead Sea fault from GPS measurements. *Journal of Geodynamics*, *67*, 30–39. <https://doi.org/10.1016/J.JOG.2012.05.006>
- Mason, P. R. D., Nikogosian, I. K., & van Bergen, M. J. (2008). Major and trace element analysis of melt inclusions by laser ablation ICP-MS. In *Laser ablation ICP-MS in the Earth sciences: Current practices and outstanding issues*, Mineralogical Association of Canada Short Course Series (Vol. 40, pp. 219–240). Vancouver: Mineralogical Association of Canada.
- Maurel, C., & Maurel, P. (1982). Étude expérimentale de l'équilibre  $Fe^{2+}$ - $Fe^{3+}$  dans les spinelles chromifères et les liquides silicatés basiques coexistants à 1 atm. *Comptes Rendus de l'Académie des Sciences de Paris*, *295*, 209–212.
- McDonough, W. F., & Sun, S.-S. (1995). The composition of the Earth. *Chemical Geology*, *120*, 223–253.
- McKenzie, D., & Bickle, M. J. (1988). The volume and composition of melt generated by extension of the lithosphere. *Journal of Petrology*, *29*(3), 625–679. <https://doi.org/10.1093/ptrology/29.3.625>
- McKenzie, D., & O'Nions, R. K. (1991). Partial melt coefficients from inversion of rare earth element concentrations. *Journal of Petrology*, *32*(5), 1021–1091. <https://doi.org/10.1093/ptrology/32.5.1021>
- McKenzie, D., & O'Nions, R. K. (1995). The source region for ocean island basalts. *Journal of Petrology*, *36*(1), 133–159.
- McQuarrie, N., & van Hinsbergen, D. J. J. (2013). Retrodeforming the Arabia-Eurasia collision zone: Age of collision versus magnitude of continental subduction. *Geology*, *41*(3), 315–318. <https://doi.org/10.1130/G33591.1>
- Meghraoui, M., Cakir, Z., Masson, F., Mahmoud, Y., Ergintav, S., Alchalbi, A., et al. (2011). Kinematic modelling at the triple junction between the Anatolian, Arabian, African plates (NW Syria and in SE Turkey). *Geophysical Research Abstracts*, *13*, EGU2011-12599.
- Meulenkamp, J. E., Wortel, M. J. R., van Wamel, W. A., Spakman, W., & Strating, E. H. (1988). On the Hellenic subduction zone and the geodynamic evolution of Crete since the late middle Miocene. *Tectonophysics*, *146*(1–4), 203–215. [https://doi.org/10.1016/0040-1951\(88\)90091-1](https://doi.org/10.1016/0040-1951(88)90091-1)
- Miyashiro, A. (1978). Nature of alkalic volcanic rock series. *Contributions to Mineralogy and Petrology*, *66*(1), 91–104. <https://doi.org/10.1007/BF00376089>
- Morgan, W. J. (1971). Convection plumes in the lower mantle. *Nature*, *230*(5288), 42–43. <https://doi.org/10.1038/230042a0>
- Muehlberger, W. R. (1981). The splintering of the Dead Sea Fault Zone in Turkey. *Yerbilimleri*, *8*, 123–130.
- Nikogosian, I. K., Elliott, T., & Touret, J. L. R. (2002). Melt evolution beneath thick lithosphere: A magmatic inclusion study of La Palma, Canary Islands. *Chemical Geology*, *183*(1–4), 169–193. [https://doi.org/10.1016/S0009-2541\(01\)00387-4](https://doi.org/10.1016/S0009-2541(01)00387-4)
- Nikogosian, I. K., Ersoy, Ö., Whitehouse, M. J., Mason, P. R. D., de Hoog, J. C. M., Wortel, M. J. R., & van Bergen, M. J. (2016). Multiple subduction imprints in the mantle below Italy detected in a single lava flow. *Earth and Planetary Science Letters*, *449*, 12–19. <https://doi.org/10.1016/j.epsl.2016.05.033>
- Nikogosian, I. K., & van Bergen, M. J. (2010). Heterogeneous mantle sources of potassium-rich magmas in central-southern Italy: Melt inclusion evidence from Roccamonfina and Ernici (Mid Latina Valley). *Journal of Volcanology and Geothermal Research*, *197*(1–4), 279–302. <https://doi.org/10.1016/j.jvolgeores.2010.06.014>

- Nisbet, E. G. (1982). The tectonic setting and petrogenesis of kamatiites. In N. T. Arndt & E. G. Nisbet (Eds.), *Komatiites* (pp. 501–520). London: Allen and Unwin. Retrieved from <https://ci.nii.ac.jp/naid/20001269330/>
- Notsu, K., Fujitani, T., Ui, T., Matsuda, J., & Ercan, T. (1995). Geochemical features of collision-related volcanic rocks in central and eastern Anatolia, Turkey. *Journal of Volcanology and Geothermal Research*, *64*(3–4), 171–191. [https://doi.org/10.1016/0377-0273\(94\)00077-T](https://doi.org/10.1016/0377-0273(94)00077-T)
- Okay, A. I., Zattin, M., & Cavazza, W. (2010). Apatite fission-track data for the Miocene Arabia-Eurasia collision. *Geology*, *38*(1), 35–38. <https://doi.org/10.1130/G30234.1>
- Parlak, O., Delaloye, M., Kozlu, H., & Fontignie, D. (2000). Trace element and Sr-Nd isotope geochemistry of the alkali basalts observed along the Yumurtalik Fault (Adana) in southern Turkey. *Yerbilimleri*, *22*, 137–148.
- Parlak, O., Kop, A., Ünlügöç, U. C., & Demirkol, C. (1998). Geochronology and geochemistry of basaltic rocks in the Karasu Graben around Kırkhan (Hatay), S. Turkey. *Turkish Journal of Earth Sciences*, *7*, 53–61.
- Parlak, O., Kozlu, H., Demirkol, C., & Delaloye, M. (1997). Intracontinental Plio-Quaternary volcanism along the African-Anatolian plate boundary, southern Turkey. *Ofioliti*, *22*(1), 111–117.
- Pearce, J. A. (2014). Immobile element fingerprinting of ophiolites. *Elements*, *10*(2), 101–108. <https://doi.org/10.2113/gselements.10.2.101>
- Pearce, J. A., Bender, J. F., de Long, S. E., Kidd, W. S. F., Low, P. J., Güner, Y., et al. (1990). Genesis of collision volcanism in eastern Anatolia, Turkey. *Journal of Volcanology and Geothermal Research*, *44*(1–2), 189–229. [https://doi.org/10.1016/0377-0273\(90\)90018-b](https://doi.org/10.1016/0377-0273(90)90018-b)
- Pearce, J. A., & Peate, D. W. (1995). Tectonic implications of the composition of volcanic arc magmas. *Annual Review of Earth and Planetary Sciences*, *23*(1), 251–285. <https://doi.org/10.1146/annurev.ea.23.050195.001343>
- Polat, A., Kerrich, R., & Casey, J. F. (1997). Geochemistry of Quaternary basalts erupted along the east Anatolian and Dead Sea Fault Zones of southern Turkey: Implications for mantle sources. *Lithos*, *40*(1), 55–68. [https://doi.org/10.1016/S0024-4937\(96\)00027-8](https://doi.org/10.1016/S0024-4937(96)00027-8)
- Portner, D. E., Delph, J. R., Biryol, C. B., Beck, S. L., Zandt, G., Özacar, A. A., et al. (2018). Subduction termination through progressive slab deformation across eastern Mediterranean subduction zones from updated P-wave tomography beneath Anatolia. *Geosphere*, *14*(3), 907–925. <https://doi.org/10.1130/GES01617.1>
- Prelević, D., Akal, C., Foley, S. F., Romer, R. L., Stracke, A., & van den Bogaard, P. (2012). Ultrapotassic mafic rocks as geochemical proxies for post-collisional dynamics of orogenic lithospheric mantle: The case of southwestern Anatolia, Turkey. *Journal of Petrology*, *53*(5), 1019–1055.
- Radivojević, M., Toljić, M., Turki, S. M., Bojić, Z., Šarić, K., & Cvetković, V. (2015). Neogene to Quaternary basalts of the Jabal Eghei (Nuqay) area (south Libya): Two distinct volcanic events or continuous volcanism with gradual shift in magma composition? *Journal of Volcanology and Geothermal Research*, *293*, 57–74. <https://doi.org/10.1016/J.JVOLGORES.2015.02.003>
- Reid, M. R., Schleiffarth, W. K., Cosca, M. A., Delph, J. R., Blichert-Toft, J., & Cooper, K. M. (2017). Shallow melting of MORB-like mantle under hot continental lithosphere, Central Anatolia. *Geochemistry, Geophysics, Geosystems*, *18*, 1866–1888. <https://doi.org/10.1002/2016GC006772>
- Richardson-Bunbury, J. M. (1996). The Kula volcanic field, western Turkey: The development of a Holocene alkali basalt province and the adjacent normal-faulting graben. *Geological Magazine*, *133*(3), 275–283.
- Ring, U., Johnson, C., Hetzel, R., & Gessner, K. (2003). Tectonic denudation of a late Cretaceous-Tertiary collisional belt: Regionally symmetric cooling patterns and their relation to extensional faults in the Anatolide belt of western Turkey. *Geological Magazine*, *140*(4), 421–441. <https://doi.org/10.1017/S0016756803007878>
- Robertson, A. H. F., Ustaomer, T., Pickett, E. A., Collins, A. S., Andrew, T., & Dixon, J. E. (2004). Testing models of late Palaeozoic-early Mesozoic orogeny in western Turkey: Support for an evolving open-Tethys model. *Journal of the Geological Society*, *161*(3), 501–511. <https://doi.org/10.1144/0016-764903-080>
- Roedder, E. (1984). Fluid inclusions. In P. H. Ribbe (Ed.), *Reviews in mineralogy* (Vol. 12, pp. 1–646). Washington, DC: Mineralogical Society of America.
- Rojay, B., Heimann, A., & Toprak, V. (2001). Neotectonic and volcanic characteristics of the Karasu fault zone (Anatolia, Turkey): The transition zone between the Dead Sea Transform and the East Anatolian Fault Zone. *Geodinamica Acta*, *14*(1–3), 197–212.
- Rudge, J. F., MacLennan, J., & Stracke, A. (2013). The geochemical consequences of mixing melts from a heterogeneous mantle. *Geochimica et Cosmochimica Acta*, *114*, 112–143. <https://doi.org/10.1016/j.gca.2013.03.042>
- Ryan, W. B. F., Carbotte, S. M., Coplan, J. O., O'Hara, S., Melkonian, A., Arko, R., et al. (2009). Global multi-resolution topography synthesis. *Geochemistry, Geophysics, Geosystems*, *10*, Q03014. <https://doi.org/10.1029/2008GC002332>
- Saal, A. E., Hart, S. R., Shimizu, N., Hauri, E. H., & Layne, G. D. (1998). Pb isotopic variability in melt inclusions from oceanic island basalts, Polynesia. *Science*, *282*(5393), 1481–1484. <https://doi.org/10.1126/science.282.5393.1481>
- Saccani, E., Allahyari, K., & Rahimzadeh, B. (2014). Petrology and geochemistry of mafic magmatic rocks from the Sarve-Abad ophiolites (Kurdistan region, Iran): Evidence for interaction between MORB-type asthenosphere and OIB-type components in the southern Neo-Tethys Ocean. *Tectonophysics*, *621*, 132–147. <https://doi.org/10.1016/j.tecto.2014.02.011>
- Saccani, E., Azimzadeh, Z., Dilek, Y., & Jahangiri, A. (2013). Geochronology and petrology of the early Carboniferous Misho Mafic Complex (NW Iran), and implications for the melt evolution of Paleo-Tethyan rifting in Western Cimmeria. *Lithos*, *162–163*, 264–278. <https://doi.org/10.1016/j.lithos.2013.01.008>
- Schiano, P., Clocchiatti, R., Ottolini, L., & Sbrana, A. (2004). The relationship between potassic, calc-alkaline and Na-alkaline magmatism in South Italy volcanoes: A melt inclusion approach. *Earth and Planetary Science Letters*, *220*(1–2), 121–137. [https://doi.org/10.1016/S0012-821X\(04\)00048-2](https://doi.org/10.1016/S0012-821X(04)00048-2)
- Şen, P. A., Temel, A., & Gourgaud, A. (2004). Petrogenetic modelling of Quaternary post-collisional volcanism: A case study of central and eastern Anatolia. *Geological Magazine*, *141*(1), 81–98. <https://doi.org/10.1017/S0016756803008550>
- Şengör, A. M. C. (1987). Tectonics of the Tethysides: Orogenic collage development in a collisional setting. *Annual Review of Earth and Planetary Sciences*, *15*(1), 213–244. <https://doi.org/10.1146/annurev.ea.15.050187.001241>
- Şengör, A. M. C., Görür, N., & Şaroğlu, F. (1985). Strike-slip faulting and related basin formation in zones of tectonic escape: Turkey as a case study. In *Strike-slip deformation, basin formation, and sedimentation*, *The Society of Economic Paleontologists and Mineralogists* (Vol. 37, pp. 227–264). Tulsa, OK: SEPM Society for Sedimentary Geology. <https://doi.org/10.2110/pec.85.37.0227>
- Şengör, A. M. C., & Kidd, W. S. F. (1979). Post-collisional tectonics of the Turkish-Iranian plateau and a comparison with Tibet. *Tectonophysics*, *55*(3–4), 361–376. [https://doi.org/10.1016/0040-1951\(79\)90184-7](https://doi.org/10.1016/0040-1951(79)90184-7)
- Şengör, A. M. C., Özeren, M. S., Keskin, M., Sakaç, M., Özbakır, A. D., & Kayan, İ. (2008). Eastern Turkish high plateau as a small Turkic-type orogen: Implications for post-collisional crust-forming processes in Turkic-type orogens. *Earth-Science Reviews*, *90*(1–2), 1–48. <https://doi.org/10.1016/J.EARSCIREV.2008.05.002>
- Şengör, A. M. C., Özeren, S., Genç, T., & Zor, E. (2003). East Anatolian high plateau as a mantle-supported, north-south shortened domal structure. *Geophysical Research Letters*, *30*(24), 8045. <https://doi.org/10.1029/2003GL017858>

- Şengör, A. M. C., & Yilmaz, Y. (1981). Tethyan evolution of Turkey: A plate tectonic approach. *Tectonophysics*, 75(3–4), 181–241. [https://doi.org/10.1016/0040-1951\(81\)90275-4](https://doi.org/10.1016/0040-1951(81)90275-4)
- Seyitoğlu, G., Anderson, D., Nowell, G., & Scott, B. (1997). The evolution from Miocene potassic to Quaternary sodic magmatism in western Turkey: Implications for enrichment processes in the lithospheric mantle. *Journal of Volcanology and Geothermal Research*, 76(1–2), 127–147.
- Shaw, J. E., Baker, J. A., Menzies, M. A., Thirlwall, M. F., & Ibrahim, K. M. (2003). Petrogenesis of the largest intraplate volcanic field on the Arabian Plate (Jordan): A mixed lithosphere–asthenosphere source activated by lithospheric extension. *Journal of Petrology*, 44(9), 1657–1679. <https://doi.org/10.1093/ptrology/egg052>
- Sobolev, A. V. (1996). Melt inclusions in minerals as a source of principle petrological information. *Petrology*, 4(3), 228–239.
- Sobolev, A. V., Hofmann, A. W., Jochum, K. P., Kuzmin, D. V., & Stoll, B. (2011). A young source for the Hawaiian plume. *Nature*, 476(7361), 434–439. <https://doi.org/10.1038/nature10321>
- Sobolev, A. V., Hofmann, A. W., & Nikogosian, I. K. (2000). Recycled oceanic crust observed in “ghost plagioclase” within the source of Mauna Loa lavas. *Nature*, 404(6781), 986–990. <https://doi.org/10.1038/35010098>
- Sobolev, A. V., & Nikogosian, I. K. (1994). Petrology of long-lived mantle plume magmatism: Hawaii, Pacific and Reunion Island, Indian Ocean. *Petrology*, 2(2), 111–144.
- Sölpüker, U. (2007). *Petrology of Kula volcanic province, western Turkey*, (Doctoral dissertation). Cincinnati, OH: University of Cincinnati.
- Steinberger, B. (2000). Plumes in a convecting mantle: Models and observations for individual hotspots. *Journal of Geophysical Research*, 105(B5), 11,127–11,152. <https://doi.org/10.1029/1999JB900398>
- Stern, R. J., & Johnson, P. (2010). Continental lithosphere of the Arabian Plate: A geologic, petrologic, and geophysical synthesis. *Earth-Science Reviews*, 101(1–2), 29–67. <https://doi.org/10.1016/J.EARSCIREV.2010.01.002>
- Stracke, A., Zindler, A., Salters, V. J. M., McKenzie, D., Blichert-Toft, J., Albarède, F., & Grönvold, K. (2003). Theistareykir revisited. *Geochemistry, Geophysics, Geosystems*, 4(2), 8507. <https://doi.org/10.1029/2001GC000201>
- Sun, S.-S., & McDonough, W. F. (1989). Chemical and isotopic systematics of oceanic basalts: Implications for mantle composition and processes. In A. D. Saunders & M. J. Norry (Eds.), *Magmatism in the Ocean Basins, Geological Society Special Publication* (Vol. 42, pp. 313–345). <https://doi.org/10.1144/GSL.SP.1989.042.01.19>
- Takahashi, E., & Kushiro, I. (1983). Melting of a dry peridotite at high pressures and basalt magma genesis. *American Mineralogist*, 68, 859–879.
- Tatar, O., Piper, J. D. A., Gürsoy, H., Heimann, A., & Koçbulut, F. (2004). Neotectonic deformation in the transition zone between the Dead Sea Transform and the East Anatolian Fault Zone, southern Turkey: A palaeomagnetic study of the Karasu Rift Volcanism. *Tectonophysics*, 385(1–4), 17–43. <https://doi.org/10.1016/j.tecto.2004.04.005>
- Taymaz, T., Yilmaz, Y., & Dilek, Y. (2007). The geodynamics of the Aegean and Anatolia: Introduction. *Geological Society, London, Special Publications*, 291(1), 1–16. <https://doi.org/10.1144/SP291.1>
- Tokçaer, M., Agostini, S., & Savaşçın, M. Y. (2005). Geotectonic setting and origin of the youngest Kula volcanics (western Anatolia), with a new emplacement model. *Turkish Journal of Earth Sciences*, 14, 145–166.
- Torsvik, T. H., Burke, K., Steinberger, B., Webb, S. J., & Ashwal, L. D. (2010). Diamonds sampled by plumes from the core–mantle boundary. *Nature*, 466(7304), 352–355. <https://doi.org/10.1038/nature09216>
- van Hinsbergen, D. J. J. (2010). A key extensional metamorphic complex reviewed and restored: The Menderes Massif of western Turkey. *Earth-Science Reviews*, 102(1–2), 60–76. <https://doi.org/10.1016/J.EARSCIREV.2010.05.005>
- van Hinsbergen, D. J. J., Dekkers, M. J., Bozkurt, E., & Koopman, M. (2010). Exhumation with a twist: Paleomagnetic constraints on the evolution of the Menderes metamorphic core complex, western Turkey. *Tectonics*, 29, TC3009. <https://doi.org/10.1029/2009TC002596>
- van Hinsbergen, D. J. J., Hafkenscheid, E., Spakman, W., Meulenkamp, J. E., & Wortel, R. (2005). Nappe stacking resulting from subduction of oceanic and continental lithosphere below Greece. *Geology*, 33(4), 325. <https://doi.org/10.1130/G20878.1>
- van Hinsbergen, D. J. J., Kaymakci, N., Spakman, W., & Torsvik, T. H. (2010). Reconciling the geological history of western Turkey with plate circuits and mantle tomography. *Earth and Planetary Science Letters*, 297(3–4), 674–686. <https://doi.org/10.1016/j.epsl.2010.07.024>
- van Hinsbergen, D. J. J., Maffione, M., Plunder, A., Kaymakci, N., Ganerød, M., Hendriks, B. W. H., et al. (2016). Tectonic evolution and paleogeography of the Kirşehir Block and the Central Anatolian Ophiolites, Turkey. *Tectonics*, 35, 983–1014. <https://doi.org/10.1002/2015TC004018>
- van Hinsbergen, D. J. J., & Schmid, S. M. (2012). Map view restoration of Aegean–West Anatolian accretion and extension since the Eocene. *Tectonics*, 31, TC5005. <https://doi.org/10.1029/2012TC003132>
- van Hinsbergen, D. J. J., Steinberger, B., Doubrovine, P. V., & Gassmöller, R. (2011). Acceleration and deceleration of India-Asia convergence since the Cretaceous: Roles of mantle plumes and continental collision. *Journal of Geophysical Research*, 116, B06101. <https://doi.org/10.1029/2010JB008051>
- Walker, D., Shibata, T., & DeLong, S. E. (1979). Abyssal tholeiites from the Oceanographer Fracture Zone. *Contributions to Mineralogy and Petrology*, 70(2), 111–125. <https://doi.org/10.1007/BF00374440>
- Weinstein, Y., Navon, O., Altherr, R., & Stein, M. (2006). The role of lithospheric mantle heterogeneity in the generation of Plio-Pleistocene alkali basaltic suites from NW Harrat Ash Shaam (Israel). *Journal of Petrology*, 47(5), 1017–1050. <https://doi.org/10.1093/ptrology/egl003>
- Westaway, R. (1994). Present-day kinematics of the Middle East and eastern Mediterranean. *Journal of Geophysical Research*, 99(B6), 12,071–12,090. <https://doi.org/10.1029/94JB00335>
- Westaway, R., & Arger, J. (1996). The Gölbaşı basin, southeastern Turkey: A complex discontinuity in a major strike-slip fault zone. *Journal of the Geological Society*, 153(5), 729–744.
- Westaway, R., Pringle, M., Yurtmen, S., Demir, T., Bridgland, D., Rowbotham, G., & Maddy, D. (2004). Pliocene and Quaternary regional uplift in western Turkey: The Gediz River terrace staircase and the volcanism at Kula. *Tectonophysics*, 391(1–4), 121–169. <https://doi.org/10.1016/j.tecto.2004.07.013>
- Willbold, M., & Stracke, A. (2006). Trace element composition of mantle end-members: Implications for recycling of oceanic and upper and lower continental crust. *Geochemistry, Geophysics, Geosystems*, 7, Q04004. <https://doi.org/10.1029/2005GC001005>
- Wilson, J. T. (1963). A possible origin of the Hawaiian Islands. *Canadian Journal of Physics*, 41(6), 863–870. <https://doi.org/10.1139/p63-094>
- Yahiaoui, R., Dautria, J.-M., Alard, O., Bosch, D., Azzouni-Sekkal, A., & Bodinier, J.-L. (2014). A volcanic district between the Hoggar uplift and the Tenere Rifts: Volcanology, geochemistry and age of the In-Ezzane lavas (Algerian Sahara). *Journal of African Earth Sciences*, 92, 14–20. <https://doi.org/10.1016/J.JAFREARSC.2013.12.001>
- Yilmaz, Y., Can Genç, Ş., Gürer, F., Bozcu, M., Yilmaz, K., Karacik, Z., et al. (2000). When did the western Anatolian grabens begin to develop? *Geological Society, London, Special Publications*, 173(1), 353–384. <https://doi.org/10.1144/GSL.SP.2000.173.01.17>

- Yurtmen, S., Guillou, H., Westaway, R., Rowbotham, G., & Tatar, O. (2002). Rate of strike-slip motion on the Amanos Fault (Karasu Valley, southern Turkey) constrained by K–Ar dating and geochemical analysis of Quaternary basalts. *Tectonophysics*, *344*(3–4), 207–246. [https://doi.org/10.1016/S0040-1951\(01\)00265-7](https://doi.org/10.1016/S0040-1951(01)00265-7)
- Yurtmen, S., Rowbotham, G., İşler, F., & Floyd, P. A. (2000). Petrogenesis of basalts from southern Turkey: The Plio-Quaternary volcanism to the north of Iskenderun Gulf. *Geological Society, London, Special Publications*, *173*(1), 489–512. <https://doi.org/10.1144/gsl.sp.2000.173.01.23>